JOURNAL OF GEOPHYSICAL RESEARCH, VOL. 114, C07020, doi:10.1029/2008JC004902, 2009

Chalk-Ex—Fate of $CaCO_3$ particles in the mixed layer: Evolution of patch optical properties

W. M. Balch,[1] A. J. Plueddeman,[2] B. C. Bowler,[1] and D. T. Drapeau[1]

Received 3 May 2008; revised 13 February 2009; accepted 12 March 2009; published 18 July 2009.

[1] The fate of particles in the mixed layer is of great relevance to the global carbon cycle as well as to the propagation of light in the sea. We conducted four manipulative field experiments called "Chalk-Ex" in which known quantities of uniform, calcium carbonate particles were injected into the surface mixed layer. Since the production term for these patches was known to high precision, the experimental design allowed us to focus on terms associated with particle loss. The mass of chalk in the patches was evaluated using the well-calibrated light-scattering properties of the chalk plus measurements from a variety of optical measurements and platforms. Patches were surveyed with a temporal resolution of hours over spatial scales of tens of kilometers. Our results demonstrated exponential loss of the chalk particles with time from the patches. There was little evidence for rapid sinking of the chalk. Instead, horizontal eddy diffusion appeared to be the major factor affecting the dispersion of the chalk to concentrations below the limits of detection. There was unequivocal evidence of subduction of the chalk along isopycnals and subsequent formation of thin layers. Shear dispersion is the most likely mechanism to explain these results. Calculations of horizontal eddy diffusivity were consistent with other mixed layer patch experiments. Our results provide insight into the importance of physics in the formation of subsurface particle maxima in the sea, as well as the importance of rapid coccolith production and critical patch size for maintenance of natural coccolithophore blooms in nature.

Citation: Balch, W. M., A. J. Plueddeman, B. C. Bowler, and D. T. Drapeau (2009), Chalk-Ex—Fate of $CaCO_3$ particles in the mixed layer: Evolution of patch optical properties, *J. Geophys. Res.*, *114*, C07020, doi:10.1029/2008JC004902.

1. Introduction

[2] Knowledge of particle production and loss rates is essential for interpreting and predicting optical and biogeochemical variability in the marine environment. The biological, chemical, and physical factors that affect vertical particle distributions in the mixed layer can be summarized as follows: (1) particle production at growth optima or upwelling regions where nutrient-rich water is uplifted into the euphotic zone [*Dugdale and Wilkerson*, 1989; *Holligan et al.*, 1984], (2) binding of organic polymers into nanogels then microgels [*Alldredge and Silver*, 1988; *Chin et al.*, 1998], (3) grazing and particle removal [*Banse*, 1994], (4) ocean physics (e.g., sinking, subduction, shear dispersion) [*Haury et al.*, 1990; *Itsweire et al.*, 1993], and (5) remineralization/dissolution of particles [*Milliman et al.*, 1999; *Sarmiento et al.*, 1990] (Figure 1).

[3] Minerogenic particles play a disproportionate role in ocean optics because of their high refractive index, which increases the efficiency of light scattering. The important role of minerals was initially hypothesized beginning with the work of *Brown and Gordon* [1974], in which small mineral particles were thought to be a potential source of unquantified backscattering. *Morel and Ahn* [1990, 1991] also suggested the potential role of minerals in accounting for "missing backscattering" in the sea. At about the same time, *Stramski and Kiefer* [1991] also suggested that mineral particles might be important scatterers in the marine environment.

[4] Calcium carbonate particles have a disproportionate impact on ocean optical properties and biogeochemistry because of (1) their high abundance in nature (1/4 of all marine sediments are made of $CaCO_3$, and typical seawater concentrations of $CaCO_3$ particles exceed hundreds per mL), (2) high refractive index (making them some of the most efficient light scatterers), and (3) high density (providing ballast for sinking organic matter). Not only is the mineral composition important for these particles, but particle size is critical to their optical properties as well. Specifically, detached coccoliths (disc-shaped scales from coccolithophores; several microns in diameter) and plated coccolithophores (spherical cells, 5–15 μm in diameter, surrounded by calcite coccoliths) have some of the largest backscattering cross sections of marine particles, which make them some of the strongest light scatterers in the sea. The only other particulate inorganic carbon (PIC) that can scatter as efficiently as coccoliths are the micron-sized

[1]Bigelow Laboratory for Ocean Sciences, West Boothbay Harbor, Maine, USA.
[2]Woods Hole Oceanographic Institution, Woods Hole, Massachusetts, USA.

0148-0227/09/2008JC004902$09.00

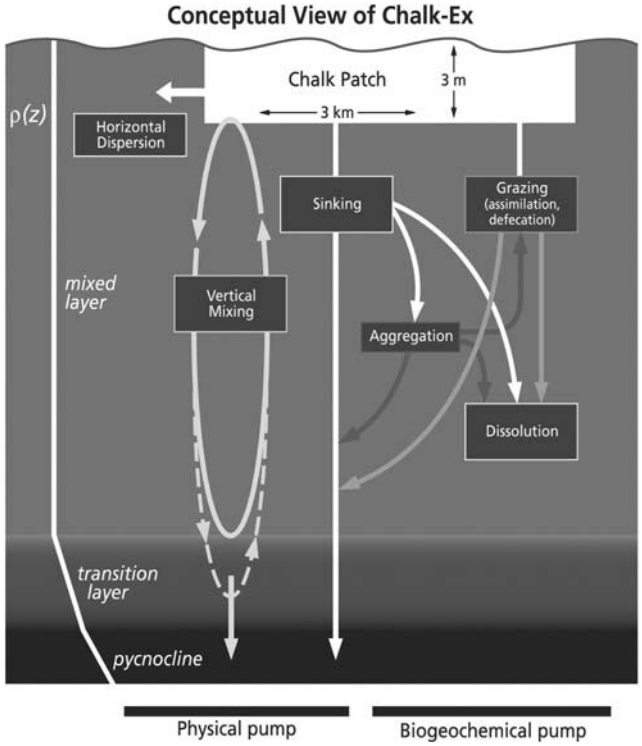

Figure 1. Conceptual view of "Chalk-Ex" experiment. Diagram shows both physical (horizontal dispersion, vertical mixing, and sinking) and biogeochemical processes (aggregation/sinking, fecal pellet repackaging/sinking, and dissolution) responsible for particle dispersion and loss from the mixed layer. Hypothetical density profile is shown at left.

aragonite particles found in relatively rare whitings that occur over carbonate banks [*Broecker et al.*, 2000; *Morse et al.*, 2003; *Robbins and Blackwelder*, 1992]. For comparison, detached coccoliths scatter orders of magnitude more light per mole PIC than do foraminifera or pteropods [*Balch et al.*, 1996b]. They also show negligible absorption of visible light [*Balch et al.*, 1991].

[5] On their own, detached coccoliths sink slowly, on the order of 0.1 m d^{-1} [*Balch et al.*, 1996c; *Honjo*, 1976]. However, when aggregated to other particles or packed into fecal pellets, they can provide important ballast to increase sinking rates of particles to hundreds of meters per day [*Honjo*, 1976]. Indeed, this is supported by the observation that the vertical flux of organic matter is well-correlated to the carbonate content of the sinking debris [*Armstrong et al.*, 2002; *Francois et al.*, 2002].

[6] Blooms of coccolithophores are common at high latitudes in early summer months [*Balch et al.*, 2005; *Brown and Yoder*, 1994; *Holligan et al.*, 1993, 1983], where PIC concentrations can reach as high as 30 μmol PIC L^{-1}, 30X the typical background concentration [*Balch et al.*, 2005]. The blooms are easily visible from space and often last for durations of 2–3 weeks. The onset of a bloom is relatively rapid as coccoliths are dropped at a late growth stage, and each cell can supply some 15–45 coccoliths. The fate of this suspended PIC is poorly understood; that is, whether the coccoliths are dispersed, slowly sink as solitary particles, aggregate and rapidly sink, are grazed and repackaged into fast sinking fecal pellets, are dissolved, etc.

[7] We here report the results of four manipulative field experiments, in which optically active $CaCO_3$ particles, the size of detached coccoliths (derived from Cretaceous coccolith chalk) were seeded into the mixed layer at two stations in the NW Atlantic, one a mesotrophic Slope station southeast of Cape Cod and one a eutrophic Shelf station in the center of Jordan Basin, Gulf of Maine. The goal of the experiments was to follow the fate of particles through the mixed layer, and this was achieved by using optically active PIC particles, the signature of which are optically unique relative to organic particles, thus they are easily traced. While the goal was not to mimic a coccolithophore bloom, the experimental results provide insights into the fate of coccolithophore blooms in nature. The experiments were done during two times of the year, June (characterized by surface warming, reduced winds, and shallow mixed layers) and November (characterized by surface cooling, increased wind forcing, and deeper mixed layers). The scientific rationale for this experiment was that by seeding a patch with a known quantity of chalk particles, the particle production term could be calculated with high precision; this would allow better quantification of the particle loss terms, under a range of conditions of external forcing and mixed layer depth.

[8] In order to assess the importance of mixed layer dynamics to vertical particle transport, the patch experiments were described in a Lagrangian framework by placing drifters inside each patch. Chalk patches were surveyed quasi-synoptically for several days, as the optical and physical properties evolved. Horizontal and vertical gradients in optical and physical properties were resolved by patch surveys with a towed, undulating Scanfish. A primary function of the surveys was to determine the three-dimensional distribution of chalk particles and to define the integrated mass of chalk within each patch. Surface forcing was determined from shipboard meteorological measurements. Vertical sinking fluxes across the base of the mixed layer were estimated with drifting sediment traps. The effects of aggregation and zooplankton grazing within the patch also were determined from a combination of laboratory and shipboard experiments (C. H. Pilskaln et al., Chalk-Ex—Fate of $CaCO_3$ particles in the mixed layer: Particle transport below the mixed layer and the role of biological and physical aggregation, submitted to *Journal of Geophysical Research*, 2009). The interaction of the chalk with dissolved organic carbon was also documented.

2. Methods

2.1. Chalk Source

[9] The source of the $CaCO_3$ for the patches was ground, Cretaceous coccolith chalk (OMYA, Dorking, Surrey, UK). The specific product (Snowcal90) had a calcium carbonate content of 97.1%, with a maximum of 2% residue, insoluble in concentrated HCl. The Snowcal90 was ground small enough to pass a 10-μm sieve (0.001% was retained on a 45-μm sieve), and the particles were randomly shaped (Figure S1a).[1] Moisture content of the chalk was 0.15%,

[1] Auxiliary materials are available in the HTML. doi:10.1029/2008JC004902.

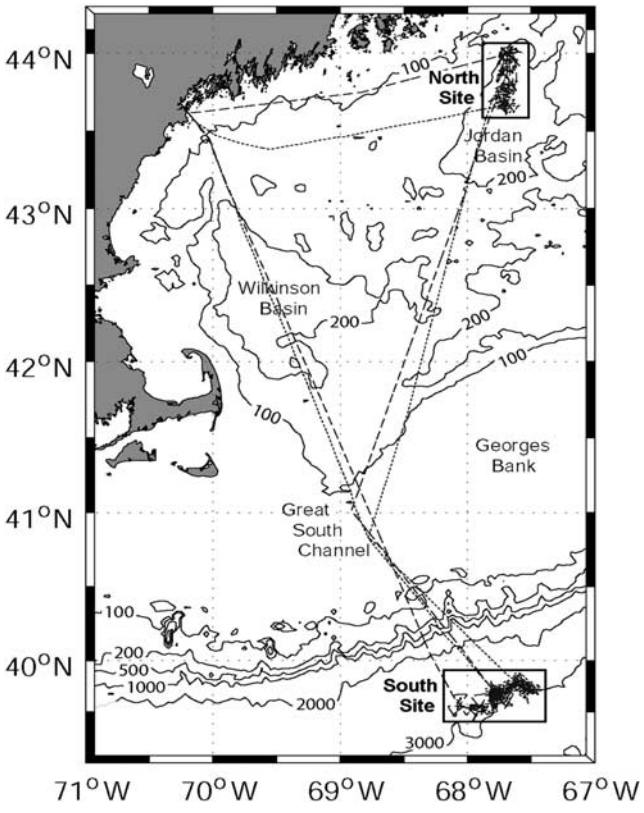

Figure 2. Map of the Gulf of Maine and Georges Bank region showing the Chalk-Ex north site and south site along with ship tracks for the 2001 (dashed) and 2003 (dotted) cruises. Bathymetry is contoured at 100, 200, 500, 1000, 2000, and 3000 m.

and the bulk material had an albedo of 89.9% for visible wavelengths. The median particle diameter was 1.92 μm, which was chosen to approximate the average size of coccoliths of *Emiliania huxleyi*.

2.2. Patch Deployment and Surveys

[10] The experiments were performed on the R/V *Endeavor* in November 2001 (cruise EN363) and June 2003 (cruise EN382). Two patches of chalk-enriched water were made during each cruise at the two sites (Figure 2). One site was 44°N 067°38′W, in Jordan Basin, Gulf of Maine (north site; patches referred to as either N′01 or N′03). The other site was over the Continental Slope, in the NW Atlantic at 39° 48′N 067° 47′W (south site; patches referred to as either S′01 or S′03). Upon reaching each site, a vertical conductivity-temperature-depth (CTD) cast was performed followed by the deployment of a "hydrodrifter" (a surface buoy with vertical array of temperature, conductivity, and current sensors) at the site which was determined to be the patch center.

[11] Patch generation always was started at dawn. Thirteen 1000-kg bags of ground Cretaceous chalk were diluted with surface seawater in two 1900-L tanks on the ship's fantail. A submersible impeller pump, capable of pumping $\sim$100 L min^{-1}, was suspended within each tank to recirculate the suspension and break up the chalk into a homogenous suspension. Initial experiments demonstrated that such recirculation was essential to eliminate chalk aggregates (which might rapidly sink). Once the chalk/seawater suspension was homogeneously mixed in the tubs, it was directed through a horizontal spreader on the ship's fantail (consisting of a 10-m-long PVC pipe with 4-mm holes every 5 cm along the entire length) that evenly dispersed the chalk/seawater mixture into the ship's wake. The chalk suspension was deployed in concentric, outward spirals around the surface drifter (Figure 3). The initial patch shape was quasi-elliptical with an area of $\sim$1.5 km^2. Because of the high reflectance of the chalk suspension, it was easy for the ship's crew to visibly locate the outer edge of the spiral during deployment, while laying the patch (with the one exception being the north site, 2001; see section 3). Two mixing tanks on the ship's stern allowed one tank to be loaded and mixed while the contents of the second tank were dispersed, minimizing the time of patch deployment to 4–5 h, in time for the daytime overpasses of SeaWiFS and MODIS ocean color satellites.

[12] Following patch deployment, floating sediment traps were also deployed (see C. H. Pilskaln et al., submitted manuscript, 2009), along with CTD/rosette casts and Scanfish surveys. A Sea-Bird Electronics CTD (model SBE-9; Bellevue, Washington, United States) was attached to the ship's rosette. The RMS error for temperature was <0.005 mdeg C, and conductivity was <0.5 μSiemens m^{-1}. The package also contained a dissolved oxygen sensor (Sea-Bird Electronics SBE-13 and SBE-23), PAR irradiance sensor (Biospherical Instruments QSP-200L4S; San Diego, California, United States), transmissometer (C-Star-25cm path; WETLabs; Philomath, Oregon, United States), and fluorometer (WetStar; WETLabs).

[13] A towed, undulating Scanfish (Chelsea Technologies Group) was used for surveying the chalk patch through time. It was equipped with a Sea-Bird CTD and an ECO Volume Scattering Function (VSF) (WETLabs) for measuring backscattering at 530 nm. Data were sampled at a frequency of 1 Hz. The Scanfish was towed at $\sim$14 km h^{-1}, with the towed sensor undulating between 5 m and a maximum depth of $\sim$100 m for the N′01 patch, 60 m for S′01 and N′03 patches, and 30 m for the S′03 patch, with an average wavelength between 0.5 and 0.75 km and ascent/descent rate of $\sim$1 m s^{-1}. In a typical Scanfish survey, the ship steamed in either a "wagon wheel" or "radiator" pattern. The survey areas were enlarged with time to better sample the patch as it dispersed. Surveys were centered on a drogued drifter, deployed immediately after chalk deployment at the patch center. The drifter consisted of dual, 10-m-long, sock-style, mesh drogues that were suspended by 1-m-long bridles beneath a surface float-line, buoyed by 20-cm-diameter floats. The drifter was designed to follow the surface mixed layer. A complete description of the drifter is given by C. H. Pilskaln et al. (submitted manuscript, 2009). When the ship made turns, the Scanfish was brought to 5-m depth for the turn and then resumed undulating once the ship resumed its new course and speed. Typical surveys lasted 3–4 h. Postcruise, the Scanfish locations were corrected according to the Lagrangian drift tracks, sampled every minute.

2.3. Underway Optical Measurements

[14] Underway surveys of inherent optical properties and hydrographic variables were made using the system de-

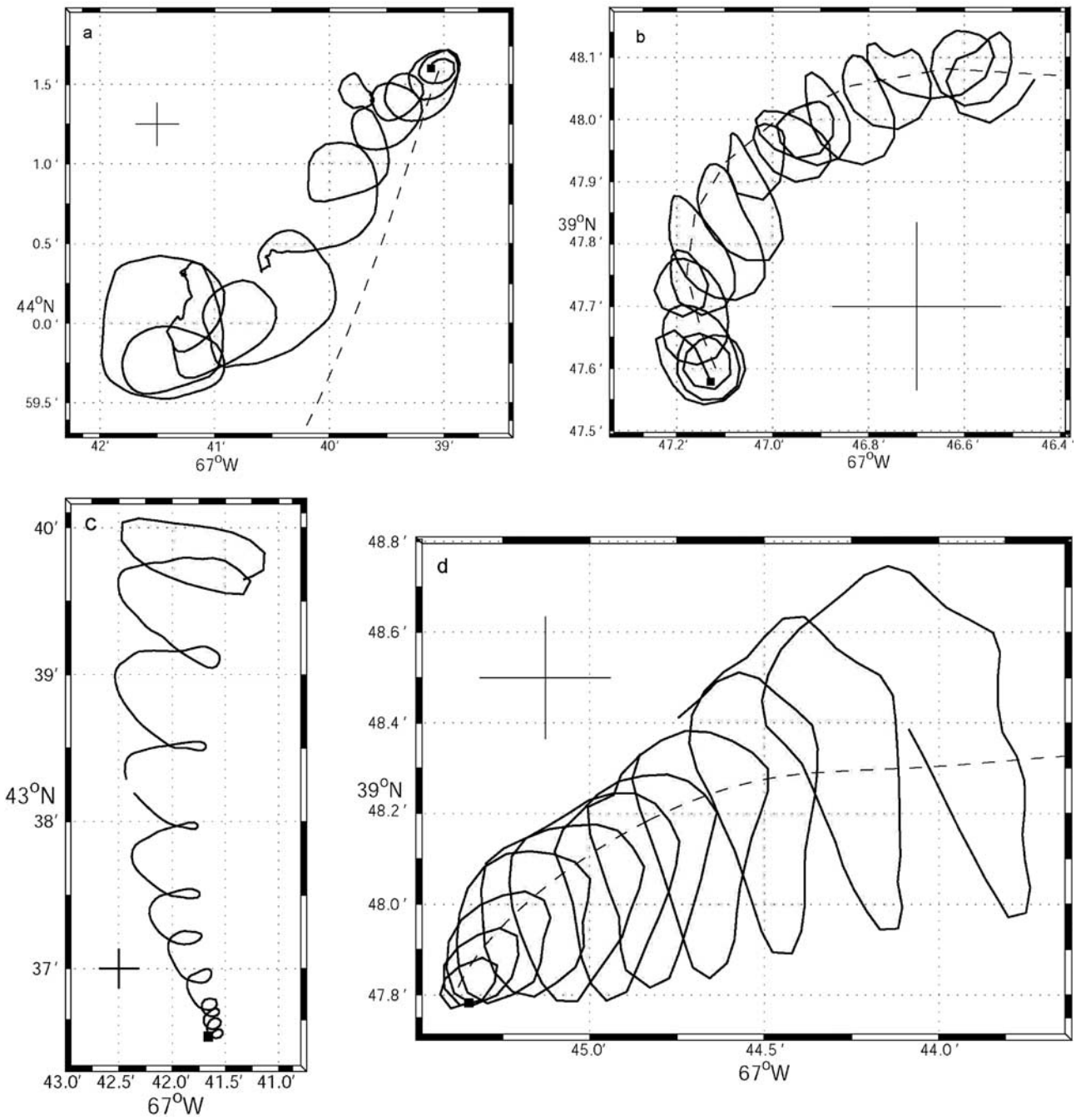

Figure 3. Ship tracks (solid lines) during chalk deployment for (a) north site 2001, (b) south site 2001, (c) north site 2003, and (d) south site 2003. A solid square marks the starting point. The track of the hydrodrifter (dashed line), used as a visual aid to navigation during chalk deployment, is also shown (track not available for north site 2003). A cross with four arms of 250 m in length is shown in Figures 3a–3d for scale. The start/end (duration) of chalk deployment operations for Figures 3a–3d was 11 November 1214–1941 UTC (7.4 h), 15 November 0958–1355 UTC (3.9 h), 13 June 0838–1323 UTC (4.7 h), and 17 June 0903–1305 UTC (4.0 h), respectively.

scribed by *Balch et al.* [2004]. The source of the water was from the ship's sea chest, with intake at 5-m depth. The continuously measured variables were salinity, temperature (Sea-Bird SBE-45 conductivity and temperature sensor), chlorophyll *a* fluorescence (Turner Designs fluorometer, calibrated to discrete chlorophyll samples [*JGOFS*, 1996]), volume scattering of 532 nm light (Wyatt Technology light-scattering photometer) integrated over scattering angles to calculate particulate backscattering (b_{bp}; m^{-1}), backscattering of acid-labile calcium carbonate (b'_b), spectral beam attenuation, and spectral absorption at nine wavelengths (WETLabs ac9) of total and 0.2-μm-filtered samples plus

spectral particle backscattering (HOBI Labs Hydroscat II sensor).

[15] A Satlantic SeaWiFS Aircraft Simulator (SAS) was used to measure above-water spectral radiance and downwelling irradiance at the sample sites. The system consisted of downlooking and sky-viewing radiance sensors, both mounted on the bow. A downwelling irradiance (E_d) sensor was mounted atop the ship's mast far from any potentially shading structures. Seven wavelengths of light were sampled from each of the SAS sensors: 412, 443, 490, 510, 555, 670, and 685 nm. Data from the three sensors were used to estimate normalized water-leaving radiance at each wavelength. The sky and water-viewing radiance sensors were set to view at 40° from zenith and nadir, respectively, as recommended by *Mueller et al.* [2003b]. The radiance sensors were able to view over an azimuth range of ±135° across the ship's bow, with no contamination from the ship's wake. The direction of the sensor was adjusted to view the water 120° from the Sun's azimuth, to minimize Sun glint. This required continually adjusting the radiometers as the Sun's and ship's position changed. Protocols for operation, calibration, and data analysis were according to *Mueller et al.* [2003a, 2003b, 2003c]. Before 1000 LT and after 1400 LT, data quality was poorer as the solar zenith angle was high. Postcruise, the 16-Hz data were filtered to remove as much residual white cap and glint as possible (we accepted only the lowest 5% of the data). Factory calibration of the sensors was performed before and after each cruise, and measurements of a calibrated reflectance plaque were made at local apparent noon on sunny days to verify the stability of radiometric calibrations. Backscattering was calculated from the above-water radiance measurements using the two-band PIC algorithm [*Balch et al.*, 2005].

2.4. Calibration of Chalk to Backscattering

[16] In order to estimate the mass balance of PIC within each patch, we empirically defined the backscattering cross section of the chalk. This first required that subsamples of chalk from each of the two batches were dried in a desiccator to remove residual moisture. Then aliquots of chalk were weighed and suspended in 0.2-μm filtered seawater for use as a primary standard. Volume scattering of serially diluted standards was measured at 18 angles in an EOS light-scattering photometer (Wyatt Technologies Corporation, Santa Barbara, California, United States). The light-scattering photometer was calibrated at 90° with a solid scattering standard supplied with the instrument. A solution of high molecular weight Dextran was used as an isotropic scattering standard to transfer the 90° detector calibration to the other angular detectors [*Balch and Drapeau*, 2004; *Balch et al.*, 2004, 1999]. The concentration of PIC was determined using an inductively coupled plasma optical emission spectrometer (ICP OES) following sampling protocol of *Fernández et al.* [1993].

[17] In order to absolutely calibrate the WETLabs ECO VSF measurements (aboard the Scanfish) to the Wyatt EOS light-scattering photometer, the two instruments were compared in the laboratory where standard chalk suspensions were put into the Wyatt EOS, or the WETLabs ECO VSF was immersed within the same standard chalk suspension. A field calibration of the two instruments was also run. This involved comparing the EOS measurements of b_{bp} (measured on seawater from the ship's flowing seawater system, taken from 5-m depth) to the b_{bp} measurements of the ECO VSF aboard the Scanfish when it was at 5-m depth. Lag correlations were used to account for the distance of the Scanfish behind the ship, the ship's speed, and the time for water to flow through the ship's underway seawater system to the EOS instrument.

2.5. Aerial Observations

[18] When weather conditions allowed, a tethered balloon was used to make high-resolution aerial observations of the patches. A 5-m helium balloon (Floatograph Technologies; Silver Spring, Maryland, United States) was towed at ~150-m altitude, with several hundred meters of Spectra® polyethylene fiber towing cable from a winch on the ship's fantail. A Sony video camera package was suspended below the balloon, and data were telemetered using a 2.2-GHz transmitter, which allowed real-time video acquisition as well as high-resolution "still" pictures to be taken remotely during deployment ("still" images were stored on board the camera and downloaded after balloon recovery). During the 2001 field campaign, the camera was equipped with a "fish-eye," wide-angle lens (18-mm focal length) to maximize the field of view. In the 2003 campaign, a standard 50-mm focal length lens was used on the camera, and the balloon tether length was adjusted in order that the ship was always visible in the video images. This allowed better geolocation of images in the 2003 cruise and improved detection of the shape of the patch and positions of its boundaries.

2.6. Statistical Calculations

[19] Chalk concentrations were quantified on the basis of calibrated particulate backscattering as described above. Because of the presence of other scattering particles in seawater (such as phytoplankton, particulate detritus, etc.), a statistical approach was used to discern waters with significant concentrations of chalk. Prior to deployment of each patch, a "prepatch" wagon wheel survey was performed with the ECO VSF (aboard the Scanfish) to measure the three-dimensional distribution of particle backscattering. The survey was centered at each planned patch site, and it had three 10-km legs placed at 60° angles from each other, with one leg oriented along the axis of the wind. Phytoplankton chlorophyll and POC concentrations in the ocean are typically lognormally distributed [*Campbell*, 1995], thus prior to performing any parametric statistics, backscattering data first were log-transformed. Significant chalk concentrations were defined according to when the backscattering was more than two standard deviations above the median prepatch backscattering value (the reason for choosing the median will be discussed further in section 3). The probability distribution for log backscattering was calculated for four vertical layers within survey of each chalk patch: (1) 1–5 m, (2) 5–13 m, (3) 13–20 m, and (4) 20–30 m. The validity of this approach for the top layer was verified independently using acid-labile backscattering, as measured aboard ship on water from 5-m depth run through the Wyatt EOS light-scattering photometer, and comparing this to the

surface backscattering as measured from the ECO VSF light-scattering photometer aboard the Scanfish.

[20] Krigging (an interpolation technique which estimates a variable at unsampled locations using weighted sums of the variable at adjoining sample points [*Deutsch and Journel*, 1992]) was performed using MATLAB Version R2006a and the WHOI/GLOBEC "easy_krig" software package Version 3.0 (available from http://globec.whoi.edu/software/kriging/easy_krig/easy_krig.html). When data were lognormally distributed, they were log transformed prior to generating the "variogram." A least squares "general Exponential-Bessel" function was used to fit to the variogram, forcing the nugget effect (estimated standard deviation of the measurement error) to be zero, thus increasing the probablility of an exact fit at measurement points. Krigging was done after this fitting process. For plan views, the krigging grid used a latitude and longitude resolution of 0.1 degrees and depth resolution corresponding to the average within each of the four depth levels (1–5 m, 5–13 m, 13–20 m, and 20–30 m). In the krigging analysis, the patch was defined as water with backscattering values two standard deviations above the median, prepatch backscattering value. Data that exceeded the krigging variance threshold (±100%) also were excluded from the final plots (typically <1% of the data).

3. Results

3.1. Calibration of PIC to Optical Backscattering

[21] The calibration of chalk concentration to total backscattering was highly linear but was significantly different between the batches of chalk used for the two cruises (Figure 4a). The best fit linear relation between PIC concentration and particulate backscattering for the 2001 chalk batch was

$$b_{bp\,\mathrm{tot}}\left[\pm 1.176 \times 10^{-3}\right] = 1.1588[\pm 0.0674]\mathrm{PIC}$$

where PIC was in units of moles PIC m^{-3} and b_{bp} was in units of reciprocal meters. Values in square brackets henceforth represent standard errors. This relationship had a squared correlation coefficient, r^2, of 0.981 (n = 4; Fstat = 154, $P < 0.02$). The best fit relation for the 2003 chalk batch was

$$b_{bp}\left[\pm 6.531 \times 10^{-4}\right] = 1.4423[\pm 0.0433]\mathrm{PIC}$$

and this relationship had a squared correlation coefficient, r^2, 0.995 (n = 4; F_{stat} = 564, $P < 0.005$).

[22] The above calibration of PIC to the EOS light-scattering photometer was traced to the ECO VSF instrument aboard the Scanfish as described in section 2. The two light-scattering devices were intercalibrated over 1.5 orders of magnitude in range of particulate backscattering. On the basis of laboratory measurements using standard chalk suspensions, the ECO VSF light-scattering photometer calibrated to within <0.01% of the EOS instrument for the

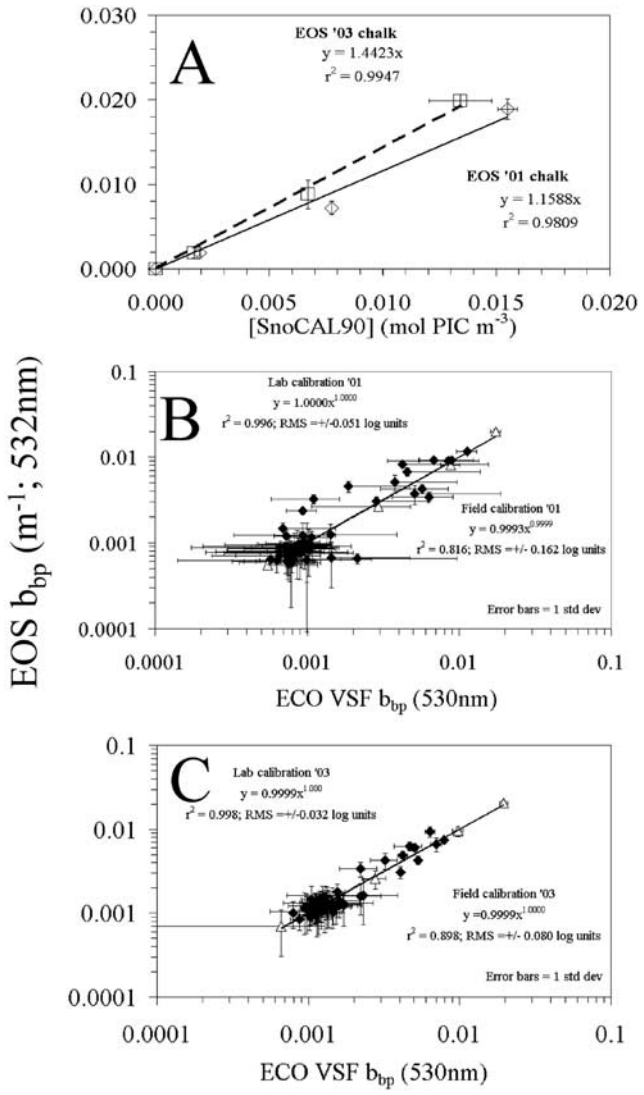

Figure 4. (a) Calibration of two batches of chalk to their backscattering as measured by the EOS light-scattering photometer. Diamonds with solid line represent total particulate backscattering corrected for seawater backscattering using the 2001 batch of SnoCal 90. Squares and dashed line represent the backscattering properties of the 2003 batch of Snowcal90. Lines are best fit power functions. Error bars represent RMS errors for five replicate samples. (b) Calibration of mean particulate backscattering (b_{bp}) values as measured by ECO Volume Scattering Function (VSF) (530 nm) and Wyatt EOS light-scattering photometer (532 nm). (c) Calibration for 2003 laboratory and field measurements. In both Figures 4b and 4c, the open triangles designate comparisons of each instrument made in the laboratory with different concentrations of suspended chalk (taken from the batches used to make the respective patches). The black diamonds represent a field comparison in which the ECO VSF was aboard the towed undulating Scanfish, and the data were subsampled when the Scanfish was at 5-m depth or shallower. Those data were then compared with the EOS backscattering measurements on water from the ship's underway system, time-lagged to account for the length of Scanfish cable deployed and the time for seawater to be pumped from the 5-m ship's intake to the EOS instrument. Error bars represent one standard error about the mean.

2001 chalk batch (r^2 = 0.996; RMS = ±0.051 log units) and within 0.01% for the 2003 chalk batch (r^2 = 0.998; RMS = ±0.032 log units) (Figure 4b; see open triangles). For the field calibration, the ECO VSF was within 0.07% of the EOS for the 2001 cruise, with higher variance (r^2 = 0.816; RMS error = ±0.162 log units). During the 2003 cruise the field backscattering measurements of the ECO VSF were within ±0.01% of the EOS instrument, and again higher variance (r^2 = 0.898; RMS = ±0.080 log units) than was observed when comparing PIC standards under laboratory conditions (Figure 4c; closed diamonds).

3.2. Discerning PIC Backscattering From Background Particulate Backscattering

[23] In order to separate chalk backscattering from background backscattering (due to other particulate matter in the seawater), we compared Scanfish ECO VSF b_{bp} data to prepatch surveys (see section 2). Probability distributions of the particle backscattering were quasi-lognormally distributed. Typically the median backscattering value was closer to the mode of the probability distribution than the mean, indicating slight skewness of the backscattering data distribution. Particle backscattering probability distributions were evaluated by comparison with prepatch distributions for each survey of each experiment. Specifically, for each postpatch survey, chalk concentrations were considered to be significantly above background for b_{bp} values greater than or equal to two standard deviations above the median prepatch b_{bp} value (e.g., Figure 5).

3.3. Narrative of Patch Observations

[24] What follows is a detailed narrative of observations for each patch. For the more general results on the mass balance of PIC over time, the reader is referred ahead to section 3.4.

3.3.1. South Patch 2001

[25] Weather conditions at the southern patch site were fair, with sunny conditions and a southeast wind of 5 m s^{-1}. The prepatch survey was begun at 0030 LT on 15 November 2001, a "wagon wheel" survey centered on the patch site, completed by 0400 LT that same day. The mixed layer (defined as the depth where the density was 0.1 sigma theta units above the surface sigma theta) in the prepatch survey was 50 m, and there was a pronounced fluorescence maximum at 20-m depth (data not shown). Chalk deployment was done between 0500 and 1000 LT. Initial patch shape was quasi-elliptical with an area of ~1.5 km^2 (Figure 3a).

[26] Backscattering probability histograms for the first postpatch survey (1222–1543 LT, 15 November; begun 2.3 h after completion of patch) indicated significant backscattering in all four layers, significantly elevated from the prepatch survey (Figure 5a). The geographical distribution of the backscattering showed that the patch was elongated with two high-backscatter lobes in the 1–5-m layer, and the b_{bp} decreased in progressively deeper levels (Figure 6a). In the 20–30-m depth layer, backscattering from chalk was barely discernable above the background. Survey 1 vertical sections (Figure 7) showed fairly uniform vertical distribution of density and deepest penetration of chalk to 19–25-m depth, with little evidence of subduction along isopycnals (but note the patch was abutting isopycnals along its long axis; see Figures 7c and 7d). Moreover, common crossover points, marked on different survey legs, illustrate that the base of the patch was moving perceptibly downward on the timescale of hours (e.g., see crossover points "a," "x," and "y" in Figure 7).

[27] In survey 2 (0301–0640 LT, 16 November 2001; ~24 h after patch deployment) there was significant backscattering from chalk between 5 and 30 m, with largest patch area between 5 and 13 m and smallest patch area in the 20–30-m layer (Figure 6b). The chalk patch still showed evidence of being elongated as in survey 1 (Figure 6). Vertical Scanfish sections from survey 2 showed clear evidence of chalk subducting northward underneath the 23.1 sigma theta isopycnal in four of the north-south survey legs (Figure 8).

[28] Survey 3 results (1747–2200 LT, 16 November 2001; ~31 h after patch deployment) demonstrated still fewer backscattering values that were significantly elevated above the prepatch survey from 5 to 30 m (Figure 5), but with the largest patch area between 13 and 20 m (Figure 6c, area 3). The patch was now broken into smaller subpatches. Vertical sections from survey 3 showed continued subduction below the 23.1 sigma theta isopycnal (Figure S2).

[29] The fourth Scanfish survey (1139–1920 LT, 17 November 2001; ~2 days after patch deployment) was prematurely terminated because of mechanical problems after one leg of the three-leg radial survey had been completed. Nonetheless, the backscattering probability distributions in all four layers showed few points significantly greater than prepatch background values (Figure 5d), and the aerial and vertical sections showed no evidence of chalk over length scales of 24 km (data not shown).

3.3.1.1. CTD Observations

[30] Beam attenuation profiles, made in conjunction with CTD profiles at the drogue marking the patch center, provided another indication of the evolution of the patch over time. Profiles from the prepatch water showed a decrease in particle beam attenuation (c_p) at the base of the mixed layer (50 m) (Figure 9a). Within 6 h of making the patch, there was high c_p from the surface down to 13 m, below which values decreased to background values (Figure 9b). There also was evidence of a subtle decrease in seawater density within this upper chalk-rich layer. A CTD profile 28 h after creation of the patch still showed peak c values above 13 m and the lower density within this surface layer (Figure 9c). The base of the mixed layer also shoaled ~10 m. At 41 h after creation of the patch, the 15-m-thick surface layer was almost 0.2 sigma theta units less dense than the water in the layer lying directly beneath it (Figure 9d). Particle beam attenuation values in the upper 30 m were still greater than the prepatch values. Below 75 m, the beam attenuation values increased ~0.02 m^{-1} from prepatch values (Figures 9a–9d).

3.3.1.2. Above-Water Observations

[31] Aerial photographs of the patch were obtained from the balloon, which was towed upwind across the patch on a southwestward course beginning 5.5 h after chalk deployment. The patch was highly elongated (Figures 10a–10e). The Langrangian drifter was at the ESE terminus of the patch along with the trap drifter (see C. H. Pilskaln et al., submitted manuscript, 2009). Thirty-meter-wide streaks were apparent in the patch, oriented roughly orthogonally to the wind (Figures 10a–10c). Three highly reflective "lobes" could be seen within the patch (Figures 10d and

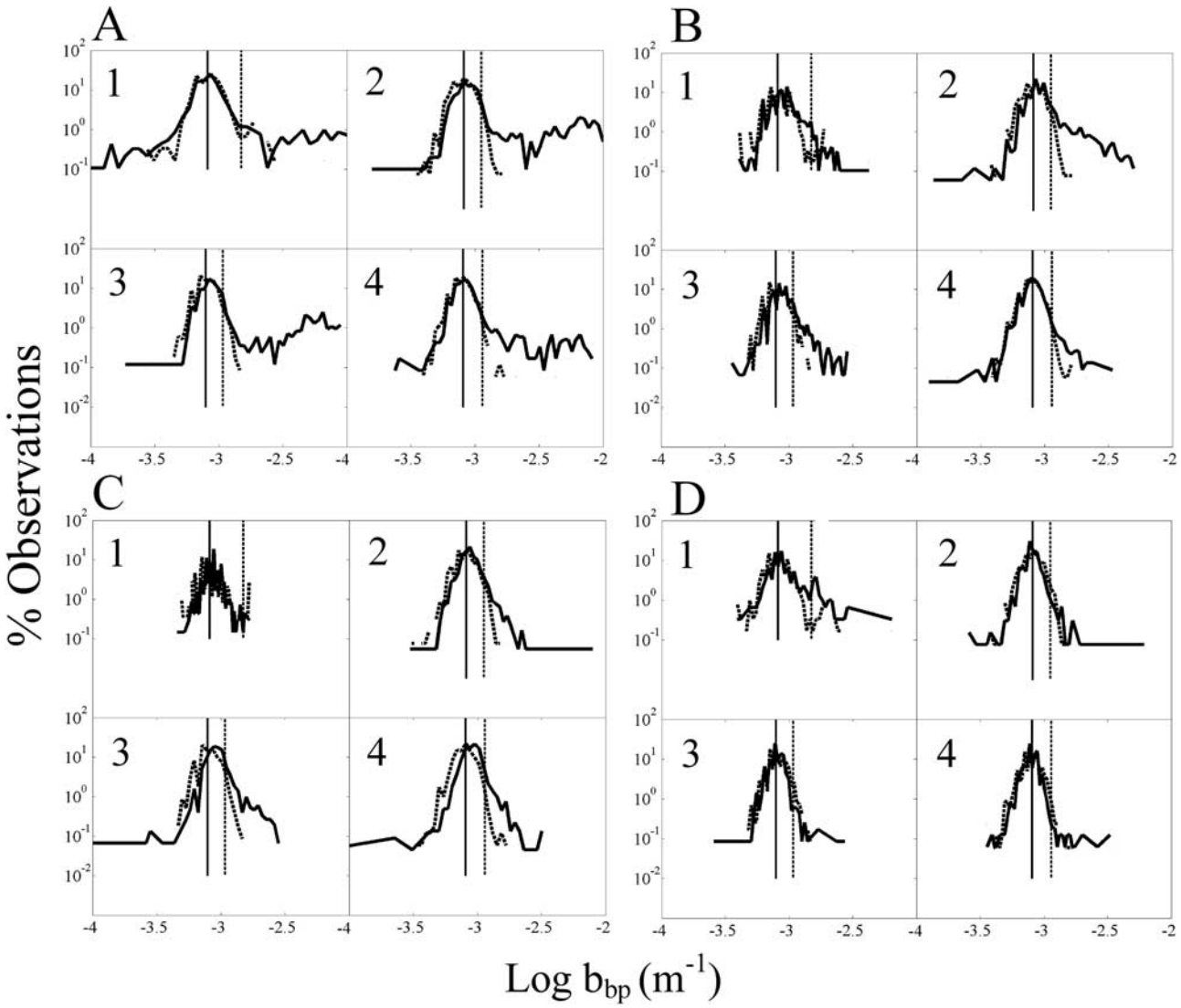

Figure 5. Backscattering probability histograms for four surveys during the S′01 chalk patch experiment. Each set of four histograms shows the results from four vertical layers in the patch: 1–5 m, 5–13 m, 13–20 m and 20–30 m. (a) (layers 1–4) Survey 1 (2–6 h after chalk deployment). (b) (layers 1–4) Survey 2 (17–19 h after chalk deployment). (c) (layers 1–4) Survey 3 (31–34.5 h after chalk deployment). (d) (layers 1–4) Survey 4 (48–52 h after chalk deployment). The solid curves represent the data distribution for the survey, and the dashed curves show the prepatch survey for reference. Patch center of each survey was estimated from vertical sock drifters set within the patch at time of patch generation. All data were subsequently Lagrangian corrected to account for patch drift. Vertical solid lines mark the median b_{bp} value for the prepatch survey. Vertical dashed lines mark two standard deviations above the median b_{bp} value. One can see the chalk being diluted and sinking through progressively deeper layers through consecutive surveys until by survey 4 (Figure 5d), the histograms are identical to the prepatch histograms.

10e). On the basis of the ship's course and speed during balloon deployment, we estimate that the patch was 2.2 km in length at the time of the aerial observations (Figure 10e).

[32] Radiance-derived backscattering values from the surface water, calculated from the first survey, showed strong covariance with backscattering at 532nm, as measured using the underway system aboard the ship (water originating from 5-m depth) (Figure 11). Backscattering estimated from above-water radiances versus EOS measurements on water from the underway system were well correlated, although the b_{bp} measured from above-water radiances were almost double the values seen in the underway water from 5-m depth (least squares power fit $y = 10.677\, x^{1.3016}$; $r^2 = 0.843$; $n = 59$, $F = 301.5$; $P < 0.001$).

3.3.2. North Patch 2001

[33] The wind conditions at the north site were ~12 m s^{-1} from the NW, and the mixed layer was ~40–60 m (Figures 9e–9i). The prepatch Scanfish survey was performed at 2247 LT on 10 November 2001. The variance in background backscattering was relatively high in all layers

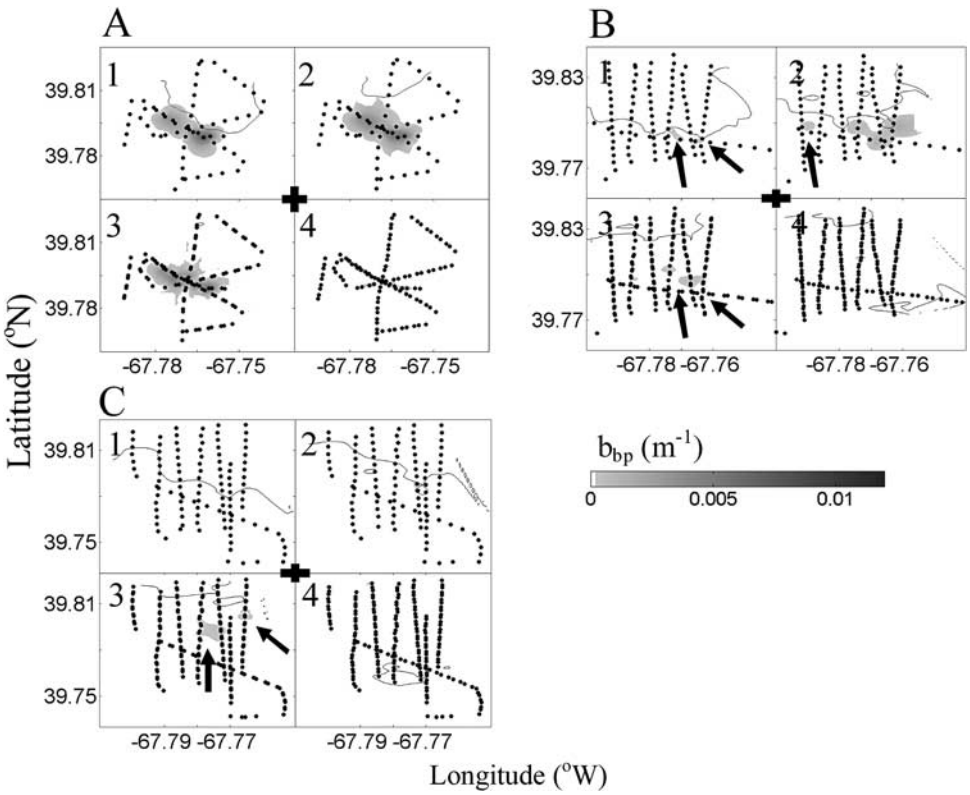

Figure 6. Aerial positions of S′01 patch. Figures 4a–4d show b_{bp} (keyed to scale bar at lower right; m^{-1}) in four layers: (layer 1) 1–5 m, (layer 2) 5–13 m, (layer 3) 13–20 m, and (layer 4) 20–30 m as measured by Scanfish. Only backscattering values greater than two standard deviations above median prepatch b_{bp} value are shown in shading. Reference "cross" at center of each survey series is a 1-km reference bar for longitude and latitude coordinates, respectively. Positions of sample points within each layer are shown as black dots. (a) Survey 1 (2.3–5.75 h after last chalk was deployed). (b) Survey 2 (17–19 h after last chalk was deployed). (c) Survey 3 (31–34.5 h after last chalk was deployed). Center of survey area was a vertical sock drifter. All data were Lagrangian corrected according to this drifter in order to correct for patch drift. Gray lines indicate isopleths of density in increments of 0.1 sigma theta units.

in the prepatch survey, with a two-peaked backscattering probability distribution, indicating two water masses with distinct optical properties within the survey area (Figure S3). During chalk deployment (0640–1400 LT, 11 November 2001; see Figure 3), it was difficult to visually detect the chalk as little as 200 m behind the ship. This was an indication that the chalk was being mixed quickly downward within the ~60-m-deep mixed layer. No chalk could be discerned statistically whether sampled (1) from PIC measurements (using ICP OES) from discrete water samples, (2) optically sampled from water taken from the CTD/Rosette, or (3) optically sampled in situ from the Scanfish. A CTD profile taken 9 h after chalk deployment showed lower c_p values throughout the water column except between 55 and 60 m where values were slightly enhanced over the prepatch profile (Figure 9f). Two CTD profiles taken near the Lagrangian drifter 37 and 40 h after chalk deployment did show beam attenuation values slightly elevated 0.03 m^{-1} from the prepatch values (Figures 9g and 9h) but we could not confirm whether this merely represented the second optical water mass observed in the prepatch survey. Fifty hours after chalk deployment, the mixed layer extended to 70 m (Figure 9i), and b_{bp} values within this layer were close to background, prepatch values. Below 70 m, 37, 40, and 50 h after chalk deployment, c_p values were higher than the prepatch or 9-h postpatch values (Figure 9).

3.3.3. South Patch 2003

[34] The wind conditions at the southern site on 16 June 2003, during the initial prepatch CTD (at 1640 LT), were 7.5 m s^{-1} from the northeast. The mixed layer was ~8 m with the pycnocline at ~28 m (Figure 9j). The chlorophyll fluorescence maximum during this prepatch CTD was within this pycnocline density gradient, situated at 37 m (data not shown). The hydrodrifter was deployed at 1815 LT, and the prepatch Scanfish survey was run in a "wagon wheel" pattern, with 10-km legs, between 1845 and 2315 LT on 16 June. The probability distribution histograms for background prepatch backscattering had a single mode and were approximately lognormal (Figure S4; dashed lines) for all vertical layers examined. The chalk patch was deployed between 0440 and 0915 LT on 17 June 2003 with decreased wind velocities 3.5–7 m s^{-1} from the ESE. The Lagrangian drifter was deployed at the patch center at 0940 LT, following creation of the patch, and two drifting sediment traps were deployed by 1035 LT on 17 June 2003.

[35] The first Scanfish survey of the chalk patch (1207–1422 LT, 17 June; see Figure S5a; ~3 h after deployment)

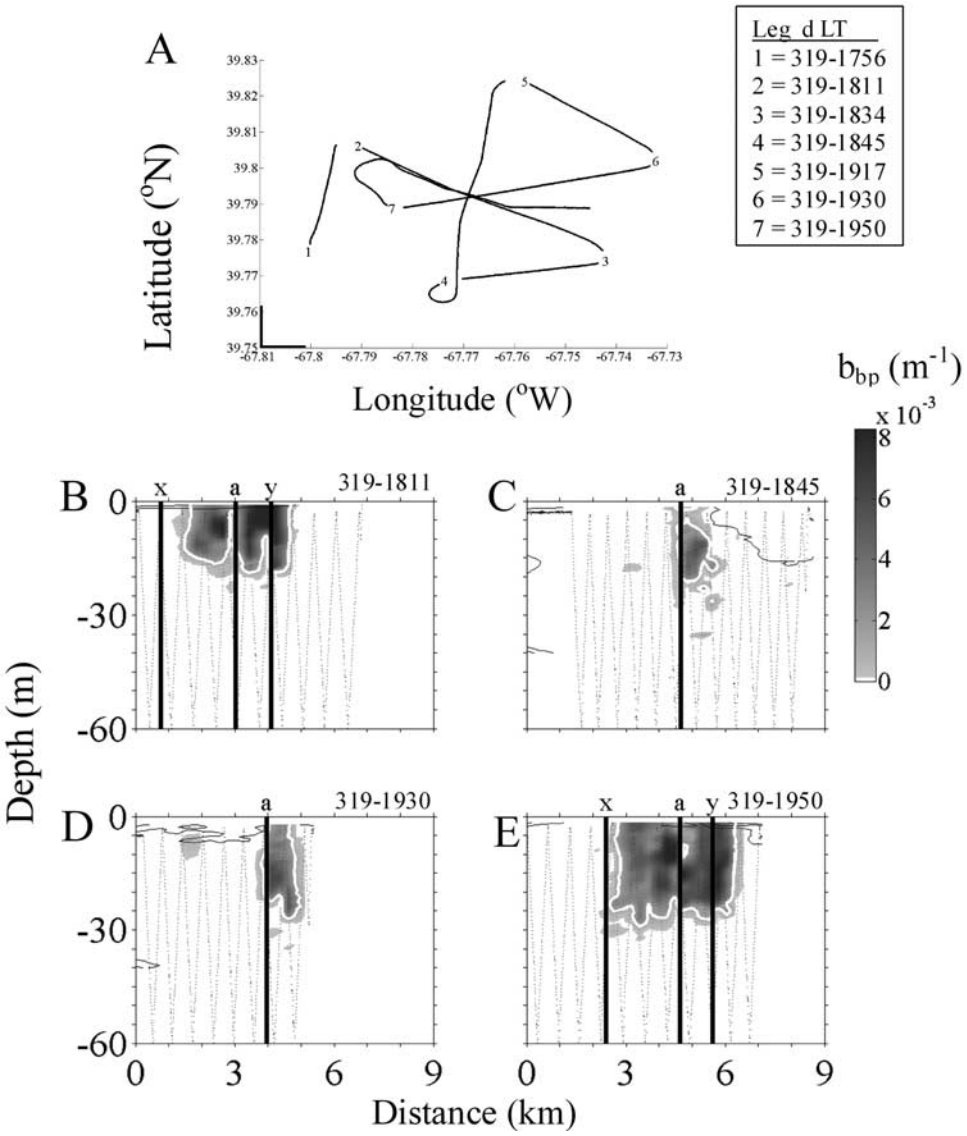

Figure 7. (a) Cruise track for Scanfish survey 1, patch S′01, showing individual legs of survey (given as calendar day, GMT start time). Numbers on cruise track mark beginning of each leg (given in key to right of Figure 7a). Figures 7b–7e show vertical sections of b_{bp} (530 nm) minus prepatch blank values for appropriate layers 1–4 (discussed in section 3.3.1). Leg number given at top right of Figures 7b–7d. Black vertical lines labeled with lower-case letters represent locations where one vertical section crossed another. (b) Leg 319–1811; crossover points and times: "a", 1821 LT, "x", 1814 LT, and "y", 1824 LT. (c) Leg 319-1845; crossover points and times: "a", 1902 LT. (d) Leg 319-1930; crossover points and times: "a", 1945 LT. (e) Leg 319-1950; crossover points and times: "a", 2005 LT, "x", 1958 LT, and "y", 2008 LT. Only data are shown where backscattering is greater than two standard deviations above prepatch median backscattering. White line represents backscattering values three standard deviations above median backscattering in prepatch survey. Density isopleths added in increments of 0.1 sigma theta unit. Position of Scanfish samples shown as small dots. Scale bar for b_{bp} with gray shading applies to Figures 7b–7e. No significant backscattering was observed in legs 1 (319-1756), 2 (319-1834), and 5 (319-1917), so these sections are not shown.

showed that the patch was not oval, but irregularly shaped in the 1–5-m layer and more expansive in the second layer (5–13 m). Low amounts of chalk penetrated to the 13–20-m layer, and no chalk was observed below 20 m. Vertical Scanfish sections from this survey (Figure 12) showed that the chalk spanned a density range of 0.2 sigma theta units over the top 15–20 m, down to the 25.3–25.5 sigma theta density isopleth (which was seen to oscillate between 15 and 20 m, with a wavelength of ~3 km).

[36] The second Scanfish patch survey (1930–2310 LT; ~10 h after deployment) was in a wagon wheel pattern, centered on the Lagrangian drifter, with one leg oriented along the SE direction of the wind (Figure S5b). No chalk could be statistically resolved in the 1–5-m layer on the

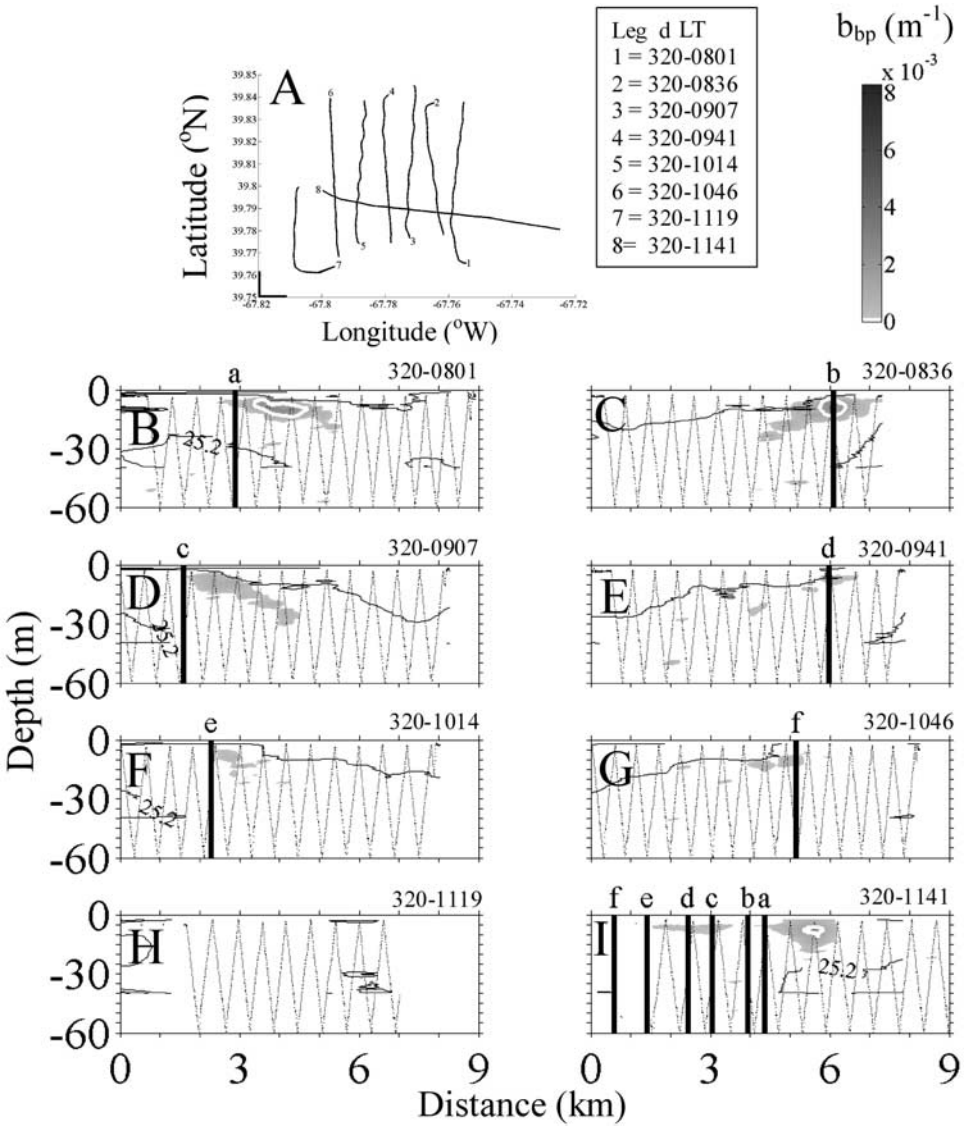

Figure 8. (a) Cruise track for Scanfish survey 2, patch S′01, showing individual legs of survey. Numbers mark beginning of each leg (given in key to right of Figure 8a). Figures 8b–8i show vertical sections of b_{bp} (530 nm) minus prepatch blank values for appropriate layers 1–4 (discussed in section 3.3.1). Leg number given at top right of Figures 8b–8i. (b) Leg 320-0801, crossover points and times: "a," 0811 LT. (c) Leg 320-0836, crossover points and times: "b," 0859 LT. (d) Leg 320-0907, crossover points and times: "c," 0913 LT. (e) Leg 320-0941, crossover points and times: "d," 1003 LT. (f) Leg 320-1014 crossover points and times: "e," 1022 LT. (g) Leg 320-1046, crossover points and times: "f," 1106 LT. (h) Leg 320-1119. (i) Leg 320-1141, crossover points and times: "a," 1156 LT, "b," 1154 LT, "c," 1151 LT, "d," 1149 LT, "e," 1146 LT, and "f" 1143 LT. All data presented as in Figure 7. Scale bar applies to Figures 8b–8i.

Figure 9. Results from sequential conductivity-temperature-depth (CTD)/transmissometer casts at each patch site. Heavy solid lines designate density (sigma theta; lower *x* axis of each plot). Fine solid lines represent beam attenuation (m^{-1}; scale on upper *x* axis of each plot). Heavy dashed line denotes a reference sigma theta and beam attenuation (660 nm) value for each patch, useful for evaluating the changes in density and beam attenuation between profiles. Time of the profile relative to the beginning of patch deployment is also given. (a–d) Density and beam attenuation profiles from S′01 patch taken 4 h prior to chalk deployment plus 6, 28, and 41 h postdeployment. Reference line corresponds to beam attenuation of 0.44 m^{-1} and sigma theta of 26.2. (e–i) Vertical profiles from N′01 patch for prepatch station −12 h, 9, 37, 40, and 50 h postpatch. Reference line corresponds to beam attenuation of 0.46 m^{-1} and sigma theta of 26.3. (j–n) Vertical profiles from S′03 patch for prepatch station −19 h and 2, 9, 15, and 22 h postpatch. Reference line corresponds to beam attenuation of 0.40 m^{-1} and sigma theta of 25.6. (o–s) Vertical profiles from N′03 patch for prepatch station −12 h and 2, 8, 16, and 31 h postpatch. Reference line corresponds to beam attenuation of 0.40 m^{-1} and sigma theta of 24.9.

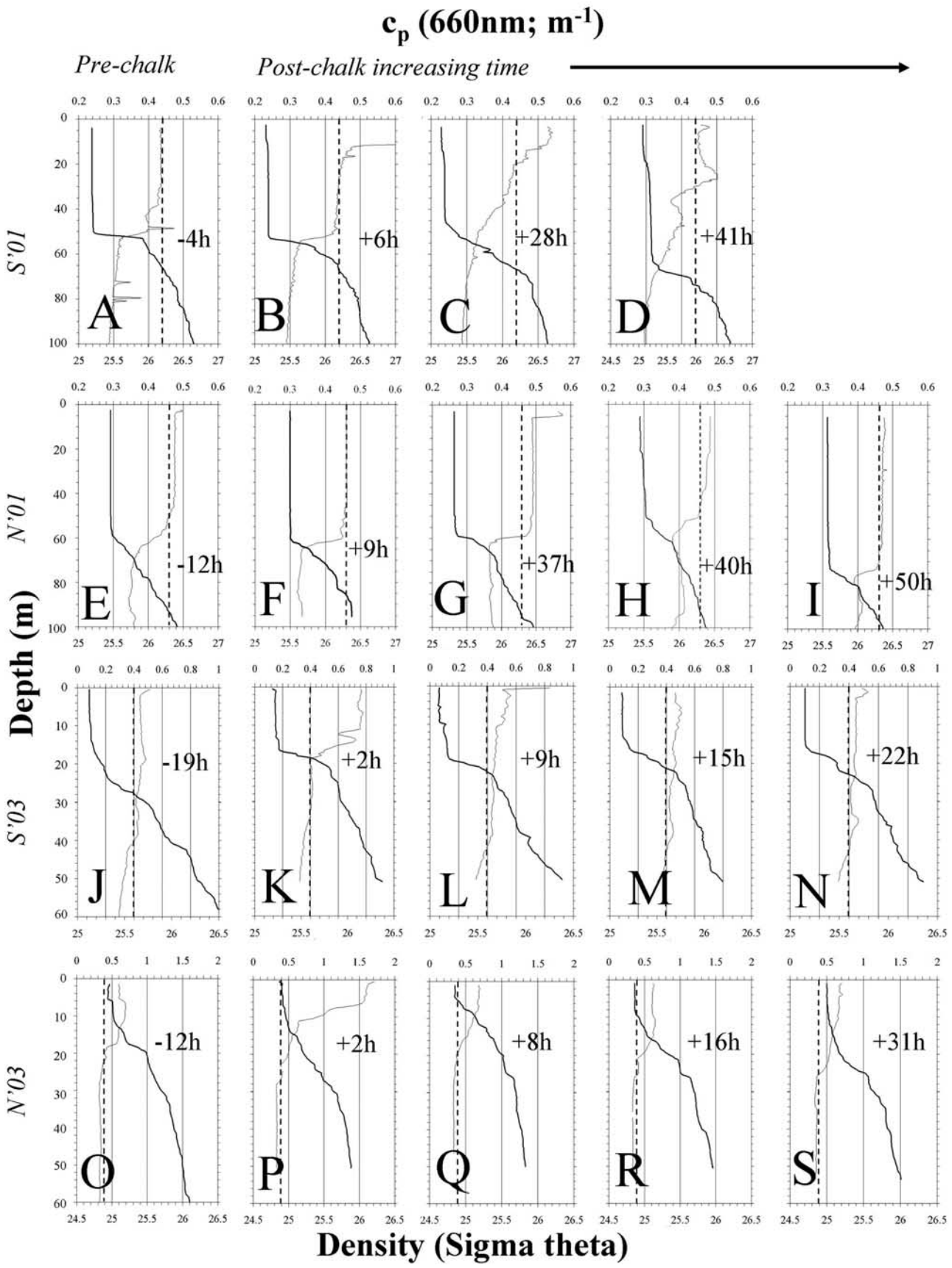
c_p (660nm; m^{-1})
Pre-chalk
Post-chalk increasing time
S'01
N'01
S'03
N'03
Depth (m)
A -4h
B +6h
C +28h
D +41h
E -12h
F +9h
G +37h
H +40h
I +50h
J -19h
K +2h
L +9h
M +15h
N +22h
O -12h
P +2h
Q +8h
R +16h
S +31h
Density (Sigma theta)

Figure 9

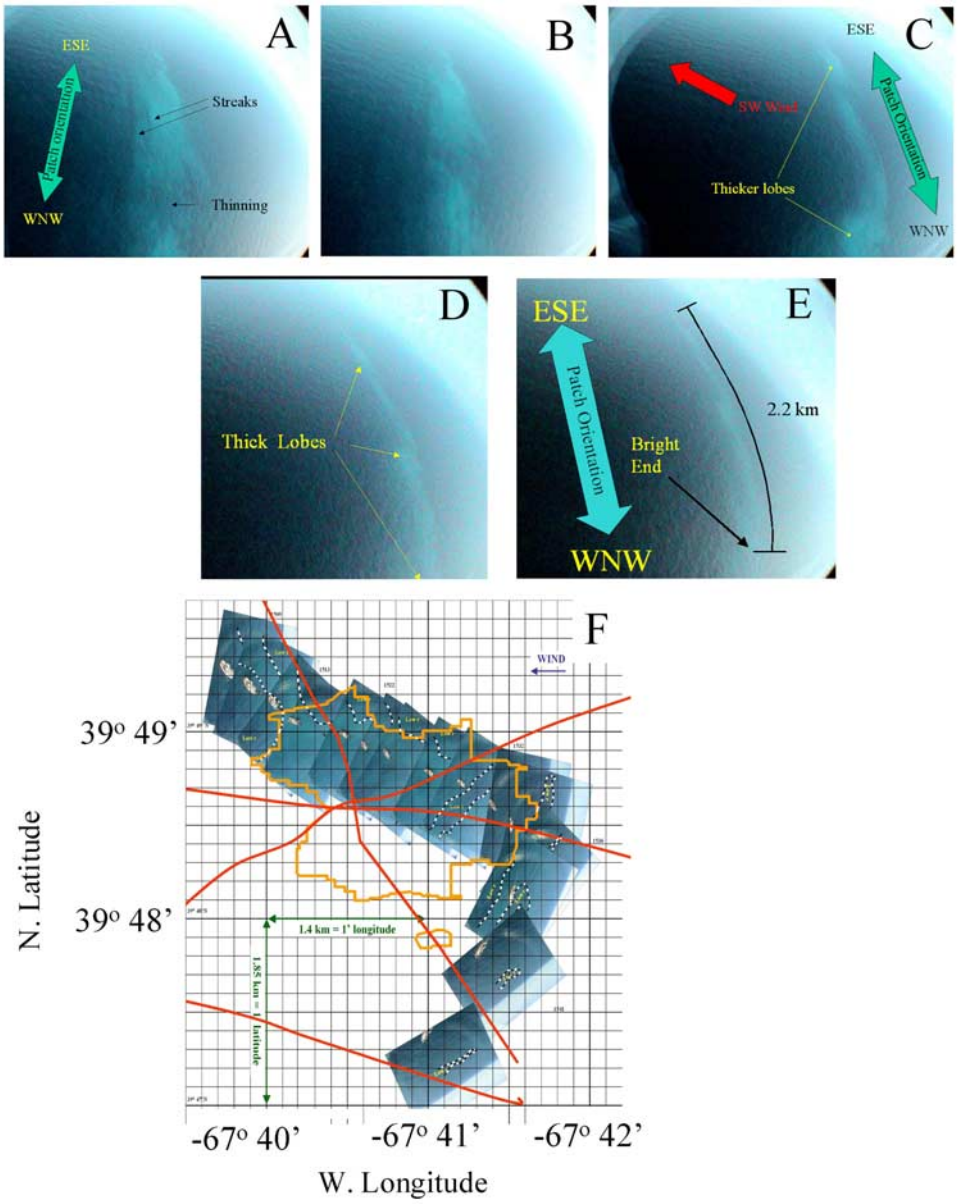

Figure 10. (a–e) Aerial views of S′01 patch. Annotations based on ship observations and cruise track during balloon deployments. Photos made with an 18-mm "fisheye" lens. The distortion of the lens, as well as absence of ship in images, made absolute navigation of images extremely difficult (hence latitude and longitude are not shown). (f) Aerial composite views of S′03 patch (started 6 h after chalk deployment). A 50-mm lens on the camera, as well as presence of ship in images, allowed absolute navigation of images. Composite images are shown on latitude/longitude coordinate grid (not corrected for Lagrangian drifter). Black and white dashed line highlights patch boundaries in each photo. Red lines show cruise track on first postpatch Scanfish survey (Figure 12a; 3 h after chalk deployment; not Lagrangian corrected). Orange line shows patch boundary as defined by krigging in first survey.

basis of the backscattering histograms (Figure S4b). Chalk was predominantly found in the 13–20-m layer with small, colocated patches in the 5–13 and 20–30-m layers (Figure S5b, areas 2–4; see arrows). The general distribution of the chalk was displaced south of the Lagrangian drifter at the center of the survey grid. Vertical sections showed that the chalk generally was between 25.3 and 25.6 sigma theta density surfaces (Figure S6) with the exception of one of the sections (Figure S6d) in which backscattering was elevated between 5 and 25 m, all in a region where the 25.2 sigma theta isopycnal domed upward from the base of the mixed layer.

[37] The third Scanfish survey was ~24 h after chalk deployment (0808–1303 LT, 18 June 2003). The only chalk found was in two 0.5-km-wide patches at the southern portion of the wagon wheel survey, at depths from 13–30 m (Figure S5c). Vertical sections revealed that the backscattering was above background levels within the pycnocline, between 25.2 and 25.6 sigma theta units (Figure 13).

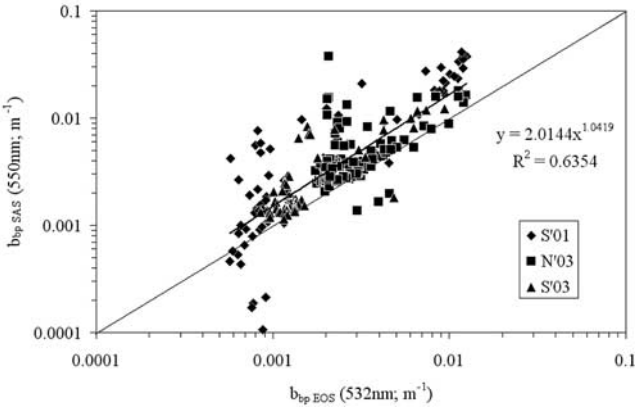

Figure 11. Plot of radiance-derived b_{bp} (550 nm; above-water radiometers, mounted on the ship's bow) versus EOS-derived b_{bp} (532 nm; using water from the ship's underway system). Backscattering data are for particles only (not including the backscattering of water). Data shown for first Scanfish surveys of the S′01 patch (diamonds), N′03 (squares), and S′03 (triangles). Thick black line is the least squares power function for the total data set. Thin black line represents 1:1 reference line.

[38] Scanfish survey 4 was run in a "radiator" pattern on 18 June from 1651 to 2145 LT (~32 h after completion of patch deployment). When integrating over each of the four layers, no significant PIC was found (Figure S5d). However, vertical sections (Figure S7) revealed several 0.5-km-wide patches between 7 and 10 m, as well as a 2.5-km patch within the pycnocline, again between 25.2 and 25.6 sigma theta units (Figure S7g). Subsequent scanfish surveys found no chalk concentrations that were significantly above the pre-patch background.

3.3.3.1. CTD Observations

[39] CTD/Transmissometer results showed that prior to patch deployment, there was a shallow mixed layer (~8 m) with uniformly low beam attenuation over the top 40 m of the water column and a slight decrease from 40 to 60 m (Figure 9j). The first profile, 2 h after patch deployment (1107 LT, 17 June), showed elevated beam attenuation from the surface to the base of the mixed layer (0–18-m depth; Figure 9k). There was some indication of layering, above and below 15 m. No chalk penetrated below 20 m. Nine hours after patch deployment, beam attenuation was significantly above prepatch values within the upper 10 m and slightly elevated down to 40 m (Figure 9l). Fifteen hours after patch deployment, slight enhancement of beam attenuation was observed from the surface to 25-m depth along with a weak local peak in attenuation near 35-m depth (Figure 9m). By 22 h after deployment (Figure 9n), attenuation in the upper 25 m was nearly uniform and not clearly elevated above background levels. A distinct local peak was observed near 35 m, indicative of chalk that had penetrated into the pycnocline.

3.3.3.2. Above-Water Observations

[40] Weather conditions allowed the surveillance balloon to be launched at 1442 LT on 17 June 2003, ~6 h after patch deployment. Wind conditions were 5 m s^{-1} from ESE; thus the aerial survey was started in the WNW corner of the survey area and run in an upwind direction. A sharp reflectance boundary was observed along the northern edge of the patch, running roughly along the axis of the wind. The northern boundary was ~3 km long, with considerable microscale patchiness in the PIC to the south (Figure 10f). Above-water measurements of normalized water-leaving radiance were converted to particulate backscattering (at 555nm) using the two-band PIC algorithm [*Balch et al.*, 2005]. Particulate backscattering estimated from EOS or radiance measurements showed a squared coefficient of correlation of 0.75, and, as with the S'01 patch measurements, the PIC was consistently overestimated but the constant and exponent of the least squares power function fit were not significantly different from 1 (Figure 11).

3.3.4. North Patch 2003

[41] The study area for the N'03 patch had a shallow mixed layer and high tidal current velocities, and it was mesotrophic in terms of the chlorophyll levels. Weather conditions at the patch site were 4.0–4.5 m s^{-1} from the west. The prepatch CTD on 13 June 2003 at 2039 LT showed that the water column had a mixed layer depth of ~6 m (Figure 9o) and bilobed fluorescence maximum between 10 and 20 m (not shown). A small peak in beam attenuation extended from 6 m to 18 m (Figure 9o). Following deployment of the hydrodrifter at 2136 LT, the prepatch Scanfish survey was run between 2220 LT on 13 June to 0143 LT on 14 June 2003 ("wagon wheel" pattern with three 10-km legs and one oriented east to west, along the axis of the wind). The probability distribution function for the prepatch backscattering had a single mode in all three layers although in the 1–5-m layer (Figure S8); the prepatch histograms of backscattering were notably broader in the 20–30-m layer than the upper layers, indicating greater variance.

[42] The chalk patch was deployed between 0504 and 0915 LT (14 June 2003). By the end of the deployment, the patch was roughly elliptical, 1.90-km long and 0.55-km wide (Figure 3c). Following deployment of the patch, two Lagrangian drifters were placed near the center of the patch (0945–1000 LT, 14 June) along with two drifting sediment traps (1000–1040 LT, 14 June).

[43] The first Scanfish survey, ~4 h after finishing patch deployment (1311–1630 LT, 14 June) showed evidence of chalk, primarily in the top layer (1–5 m) with only a small amount in the second layer (5–13 m) and none below 13 m (Figure S9a). The center of the chalk patch in the top 5 m corresponded to the center of the first Scanfish survey (Figure S9a, area 1). In layer 2, a smaller patch fell directly below the surface patch (Figure S9a, area 2). There was no obvious link between the horizontal distribution of the chalk and the density field. Vertical sections from survey 1 verified that the chalk was largely confined to the upper 5 m, in a 2.5–3-km-long patch (Figure 14). One of the legs of survey 1 (164–1806; Figure 14c) passed a crossover point ("e") at 1820 LT where the patch penetrated to ~10 m. Position "e" was recrossed during another leg (164–1852) at 1937 LT (Figure 14d), where a 0.5-km-wide patch with high backscatter extended from the surface to 22-m depth. If this patch was the same chalk previously observed at 12-m depth (Figure 14c), it would imply a vertical descent rate of 10 m in 40 min or 360 m d^{-1}.

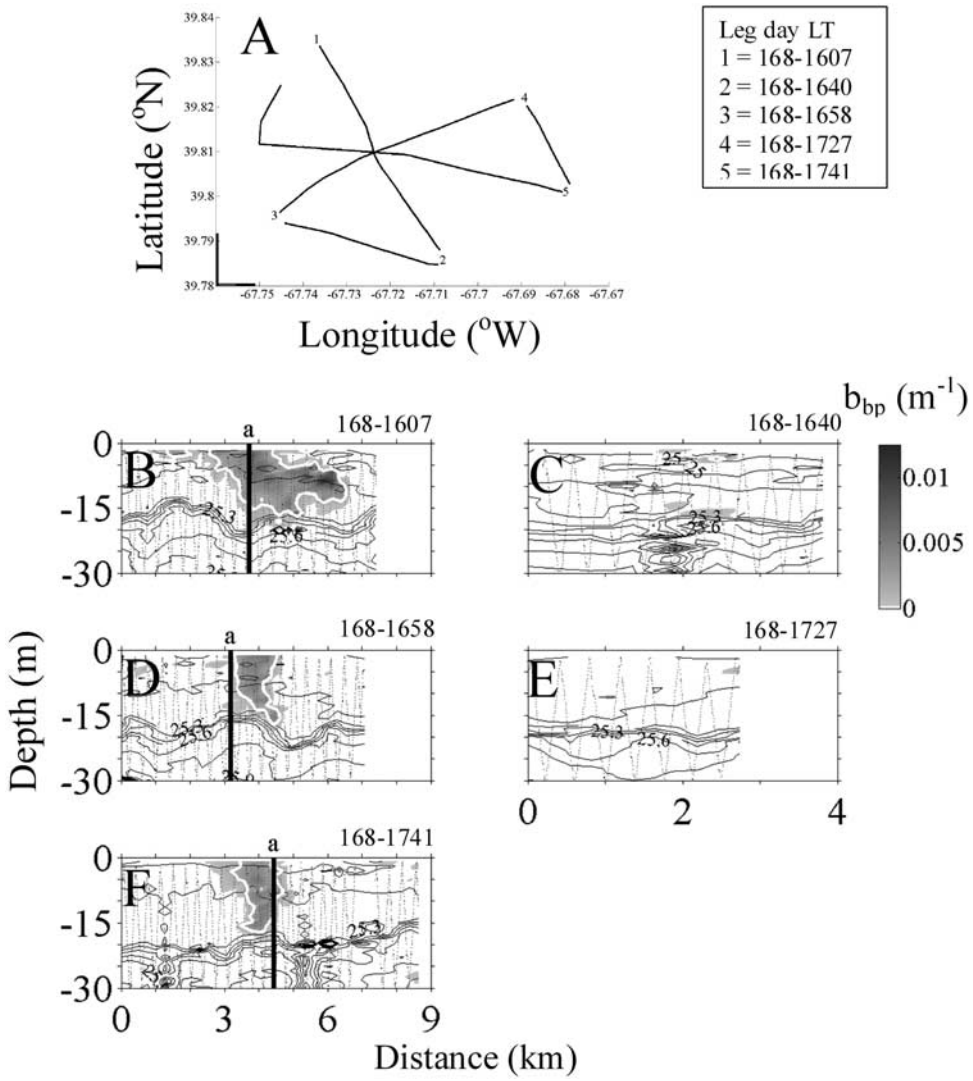

Figure 12. (a) Cruise track for Scanfish survey 1, patch S′03, showing individual legs of survey. Figures 12b–12f show vertical sections of b_{bp} (530 nm) minus prepatch blank values for appropriate layers 1–4 (discussed in section 3.3.3). Leg number given at top right of Figures 12b–12f. (b) Leg 168-1607, crossover points and times: "a," 1624 LT. (c) Leg 168-1640. (d) Leg 168-1658, crossover points and times: "a," 1711 LT. (e) Leg 168-1727. (f) Leg 168-1741, crossover points and times: "a," 1801 LT. All data presented as in Figure 7.

[44] The second Scanfish survey (2118 LT, 13 June to 0032 LT, 14 June), was begun about 12 h after the completion of patch deployment. It showed little indication of chalk when backscattering values were viewed in histograms (Figure S8b), with the exception being modest elevation above background levels for layer 2 (5–13 m) and layer 4 (20–30 m) (Figure S8b, area 2). When backscattering values were averaged over any of the four depth layers and viewed aerially (Figure S9b), no chalk was evident. Nonetheless, in two of the vertical sections (165–0131 and 165–0155), some chalk was observed above the 24.9 sigma theta isopycnal (11–14 m) (Figures S10b and S10c).

[45] The third Scanfish survey (0858–1308 LT, 14 June 2003; begun about 24 h after patch deployment) was in a wagon wheel pattern with one leg oriented north to south, along a line onto which all the Lagrangian drifters were now located. Again, the histograms of backscattering data showed little indication of chalk. Only in layer 2 (5–13 m) was there significantly elevated PIC (Figure S8c, area 2). When backscattering values within the four layers were averaged and viewed aerially, no chalk was evident (Figure S9c). However, vertical sections from the third Scanfish survey did show evidence of chalk on the eastern side of the survey area above 11 m (Figure S11). With the exception of leg 165–1544, which showed a 2.5- km coherent patch (Figure S11e), the other patches were smaller, and data from crossover points showed that the small patches were transient (i.e., they were not reproduced at crossover point "a" in Figures S11b and S11d).

[46] The fourth Scanfish survey (1520–2000 LT, 14 June) was in a "radiator" pattern, begun ~30 h after patch deployment (Figure S9d). Histograms of backscattering data were qualitatively similar to those from the third survey, and

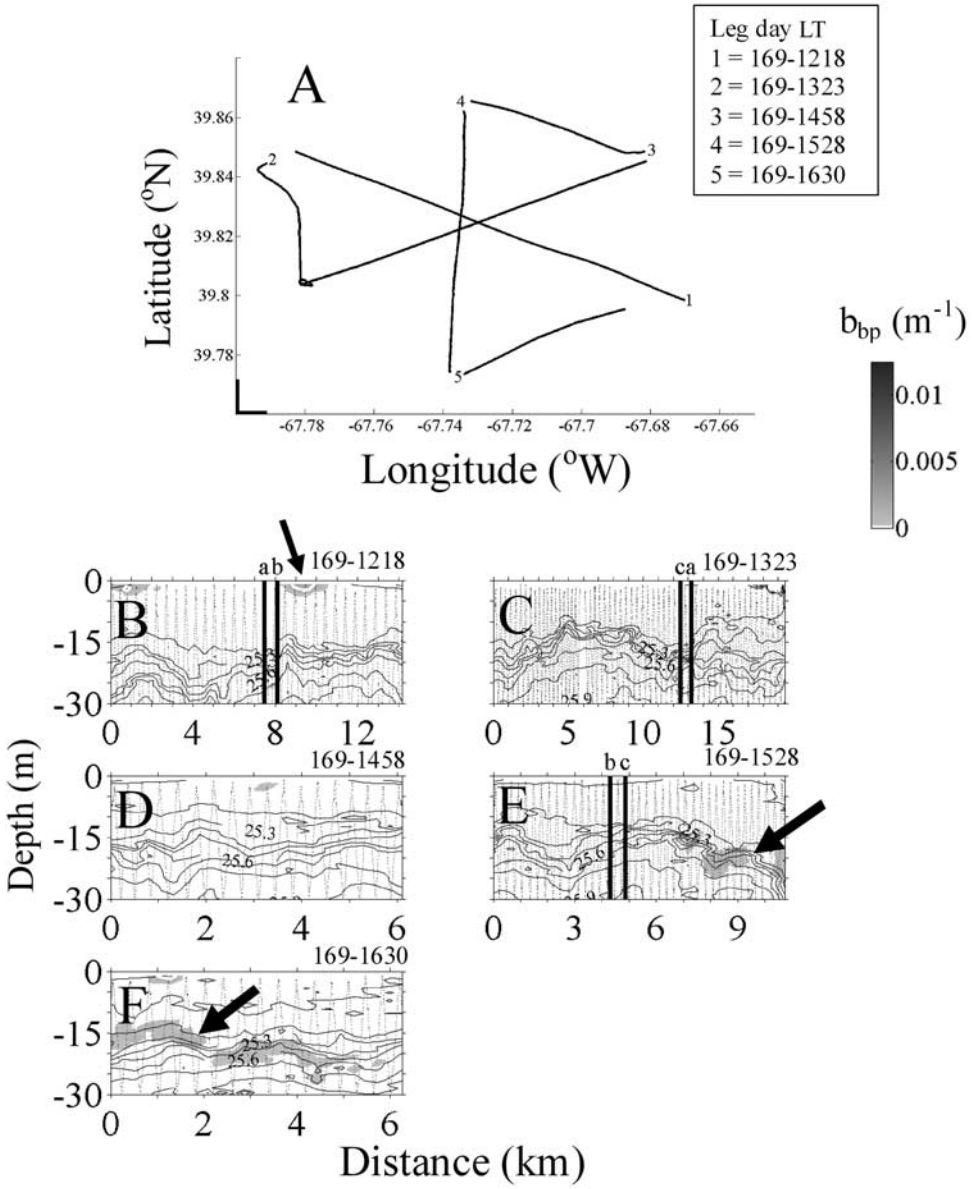

Figure 13. (a) Cruise track for Scanfish survey 3, patch S′03, showing individual legs of survey (given in key to right of Figure 13a). Figures 13b–13f show vertical sections of b_{bp} (530 nm) minus prepatch blank values for appropriate layers 1–4 (discussed in section 3.3.3). Leg number is given at top right of Figures 13b–13f. (b) Leg 169-1218, crossover points and times: "a," 1252 LT, "b," 1254 LT. (c) Leg 169-1323, crossover points and times: "c," 1426 LT and "a," 1429 LT. (d) Leg 169-1458. (e) Leg 169-1528, crossover points and times: "b," 1551 LT and "c," 1555 LT. (f) Leg 169-1630. All data presented as in Figure 7. Arrows point to layers of elevated particulate inorganic carbon (PIC) b_{bp}.

again showed no indication of chalk except in the 5–13-m layer (Figure S8d). In plan view, the layer-average backscattering was only significant in the western portion of the sample area, within layers 1 (1–5 m) and 2 (5–13 m) (Figure S9d; see arrows). Vertical sections from survey 4 revealed two closely spaced, high-scattering patches, extending a total of ~4.5 km (leg 165–2023; see Figure 15d), generally distributed from the surface to as deep as 20 m and between 24.9 and 25.1 sigma theta isopycnals. A 2.2-km patch with significant backscattering was observed shallower than 14 m during another leg of survey 4 (leg 165–2023; see Figure 15e).

[47] A fifth Scanfish survey was performed between 1302 and 1635 LT, 15 June 2003, some 52 h after completion of patch deployment. The most common backscattering values in all four layers (i.e., the modes of the probability distributions in all four layers) were less than the prepatch surveys (data not shown). This suggests that the background backscattering distribution had changed from the prepatch survey. Nevertheless, no chalk was detectable using our statistical technique.

3.3.4.1. CTD Observations

[48] The first CTD profile in the patch (1125 LT, 13 June; ~2 h after patch deployment) showed significant enhance-

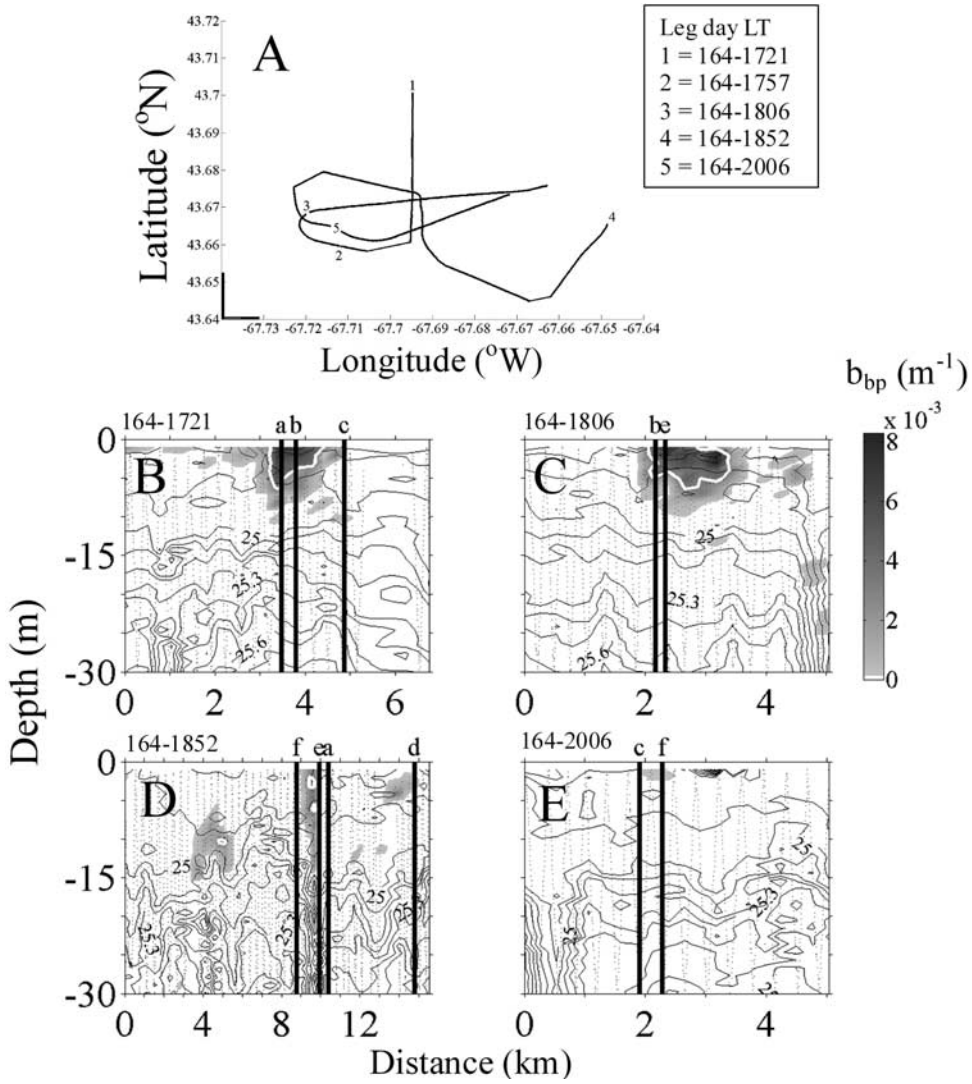

Figure 14. (a) Cruise track for Scanfish survey 1, patch N′03, performed ~4 h after patch deployment, showing individual legs of survey (given to right of Figure 14a). Figures 14b–14e show vertical sections of b_{bp} (530 nm) minus prepatch blank values for appropriate layers 1–4 (discussed in section 3.3.4). Leg numbers given at top left of Figures 14b–14e. (b) Leg 164-1721, crossover points and times: "a," 1738 LT, "b," 1740 LT. (c) Leg 164-1806, crossover points and times: "b," 1819 LT and "e," 1820 LT. (d) Leg 164-1852, crossover points and times: "f," 1932 LT, "e," 1937 LT, "a," 1939 LT, and "d," 2002 LT. (e) Leg 164-2006, crossover points and times: "c," 2016 LT and "e," 2018 LT. No significant scattering was observed in leg 2 (164-1757), so this section is not shown.

ment of beam attenuation above the background, up to values of 1.7 m^{-1} within the upper mixed layer (top 7 m; see Figure 9p). No evidence of chalk could be seen below this depth. The second CTD profile (1701 LT, 13 June; 8 h after patch deployment) revealed a somewhat shoaled mixed layer (to 5-m depth), within which beam *c* values were slightly above background (Figure 9q). The third CTD (0032 LT, 14 June; ~16 h after patch deployment) showed still lower beam *c* values (barely discernable from prepatch background values) and a mixed layer of 10 m (Figure 9r). The fourth postpatch CTD next to the Lagrangian drifter (reputed patch center) was done at 1404 LT on 14 June (~31 h after patch deployment) and demonstrated that beam *c* values at 18–25 m were above the prepatch background levels (Figure 9s).

3.3.4.2. Aerial Observations

[49] The balloon survey on the north patch was done between 1850 and 1941 LT (13 June; 9.5 h after patch deployment), and because of low Sun angles, the patch was not visible. A second balloon survey was done between 1001 and 1137 LT on 15 June (~2 days after patch deployment), and no high-reflectance water was observed (data not shown for either deployment). Particulate backscattering based on above-water radiance data was well-correlated to the EOS b_{bp} (532 nm) measurements made on water from 5-m depth (Figure 11).

3.4. Mass Balance of PIC and Patch Length Scales

[50] The mass balance of the chalk within each layer of each patch was estimated from the Scanfish data, krigged as

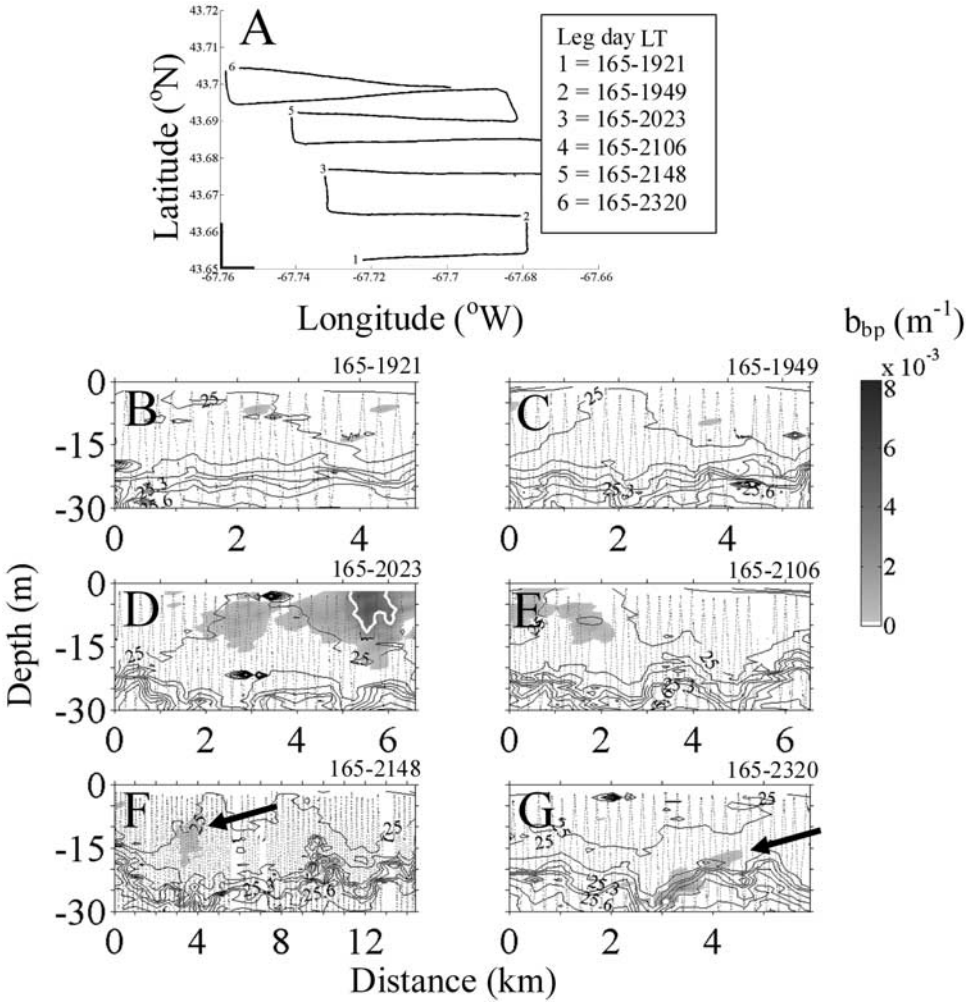

Figure 15. (a) Cruise track for Scanfish survey 4, patch N′03, showing individual legs of survey (given to right of Figure 15a). Figures 15b–15g show vertical sections of b_{bp} (530 nm) minus prepatch blank values for appropriate layers 1–4 (discussed in section 3.3.4). Leg numbers given at top right of Figures 15b–15g. (b) Leg 165-1921. (c) Leg 165-1949. (d) Leg 165-2023. (e) Leg 165-2106. (f) Leg 165-2148. (g) Leg 165-2320. All data presented as in Figure 7. Arrows indicate regions of significant particulate backscattering of background. All times are LT.

described above, where b_{bp} was run through the calibration equations (Figure 4) to estimate chalk mass. Layer integrals were summed to estimate the entire mass of chalk within each patch. The mass of chalk accounted for by each Scanfish survey dropped exponentially as a function of time (Table 1 and Figure 16a). The first postpatch surveys N′01, S′01, N′03, and S′03 (~10, 2, 3, and 4 h after patch deployment) accounted for 0%, 87%, 9% and 44% of the 13,000 kg of chalk, respectively. Ten to twenty hours after patch deployment, the respective percentages in each patch were 0%, 14%, 2%, and 6%. The rate of loss of chalk at N′01 could not be determined because from the time of deployment to the time of the initial optical measurements of any type, no chalk was detectable. For the other three patches, the specific loss rates were exponential and translated to $-0.22\ h^{-1}$ ($-5.3\ d^{-1}$) for N'03 and $-0.11\ h^{-1}$ ($-2.6\ d^{-1}$) for both S′01 and S′03.

[51] Length scales of patches were easily defined at patch deployment using the ship's navigation data (Figure 3). The chalk was deployed beginning at the patch center and spiraling outward, thus providing an accurate time and GPS position for measuring patch size. For postpatch surveys, the length scales of the major and minor axes of the patches (Table 2) were derived from the vertical Scanfish sections of b_{bp} (exceeding the prepatch median + two standard deviations) (Figures 7, 8, 12–15, S2, S6, S7, S10, and S11). It can be seen that the length scales of the patches did not uniformly increase, but showed increases over the first few hours, then decreased with time (Figures 16b–16d).

4. Discussion

[52] The most striking result of Chalk-Ex was the rapidity with which the kilometer-sized chalk patches in the mixed layer became undetectable, even under weakly forced, stratified conditions. This could have been due to a number of mechanisms outlined in section 1: (1) vertical mixing, (2) horizontal eddy diffusion of particles beyond our study

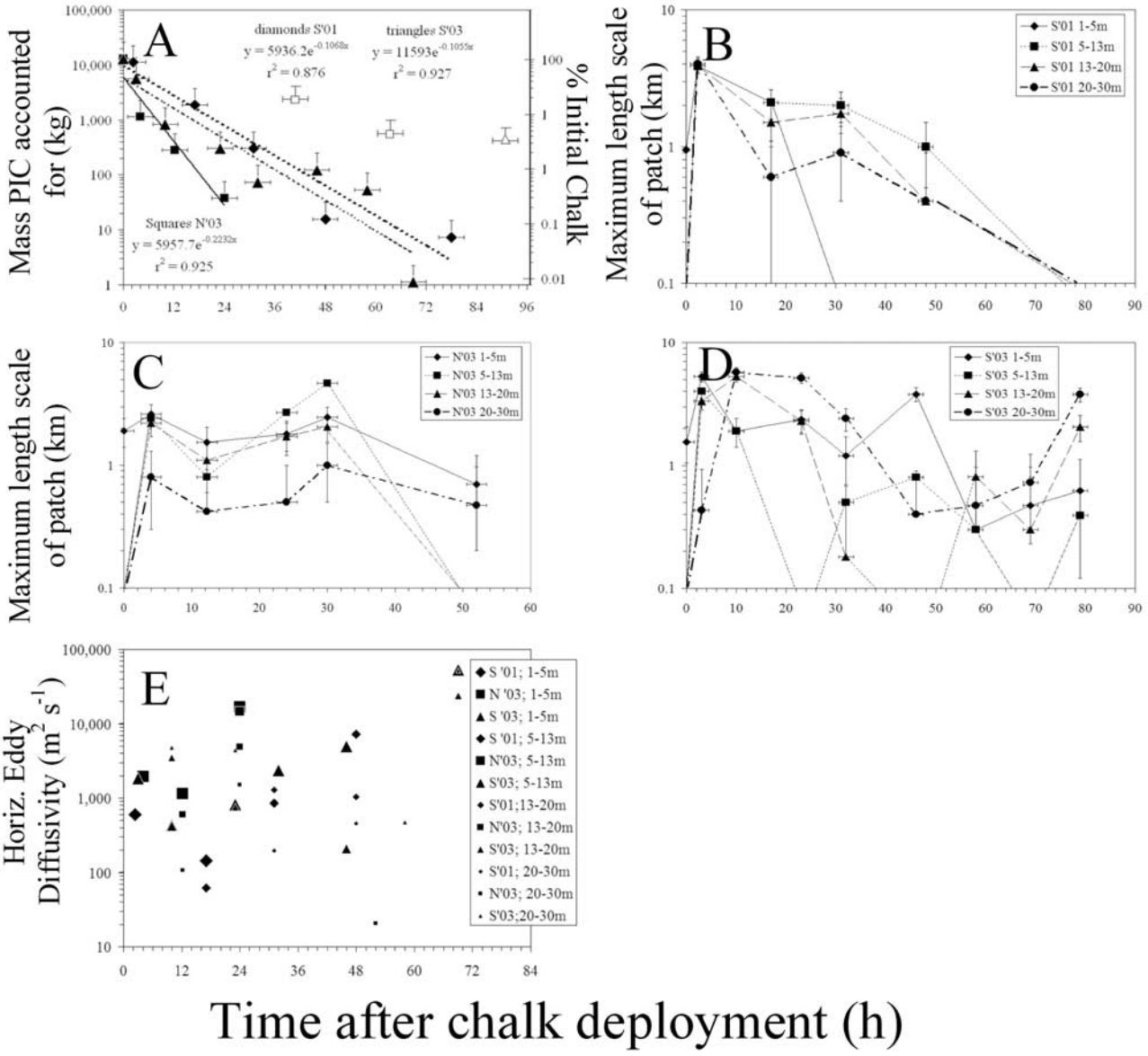

Figure 16. (a) Mass of chalk accounted for three patches, S′01, N′03, and S′03, as a function of the time of each Scanfish survey. Horizontal error bars represent the range in times over which the Scanfish survey was done. The *y* error bars represent the ±100% krigging error for the contouring (above this error, the data were not shown). Integral PIC mass derived from aerial plots (with four layers between 1-m and 30-m depth). Symbols are as follows: solid diamonds, S′01; solid squares, N′03; solid triangles, S′03. Open symbols represent surveys where the total mass of PIC increased from the previous time point and is not included in the regressions. (b) Maximum length scales from S′01 patch. Horizontal error bars same as in Figure 16a. Vertical error bars represent error in length determination (0.5 km) on the basis of Scanfish wavelength of undulation. Patch lengths <0.1 km indicate no patch was visible. Diamonds, 1–5 m; squares, 5–13 m; triangles, 13–20 m; diamonds, 20–30 m. (c) Maximum length scales from N′03 patch. Same symbols and error bars as in Figure 16b. (d) Maximum length scales from S′03 patch. Same symbols and error bars as in Figure 16b. (e) Horizontal eddy diffusivity for same three patches, same symbols as in Figure 16a. Symbol size decreases with depth. Eddy diffusivity calculation based on area of patches (major × minor axes) divided by the time after patch was deployed, normalized by the fraction of chalk not accounted for. See section 3.4 for details.

area, (3) particle sinking below the depth of observation, (4) aggregation, (5) grazing, and (6) dissolution (Figure 1). C. H. Pilskaln et al. (submitted manuscript, 2009) discuss mechanisms 1–6 in more detail. We will focus on the physical mechanisms of patch dispersal (mechanisms 1 and 2) based on the distribution of the chalk relative to the density field. Issues of experimental design and analysis that are important to interpretation of results are

Table 1. Mass Balance of PIC Accounted for in Each Patch[a]

Year	Patch	Survey	Layer (0–5 m) (kg $CaCO_3$)	Layer (5–13 m) (kg $CaCO_3$)	Layer (13–20 m) (kg $CaCO_3$)	Layer (20–30 m) (kg $CaCO_3$)	Layer (0–30 m) (kg $CaCO_3$)	Percent Accounted for
2001	north	0	322	777	401	562	2,063	15.87
2001	north	3	0	0	0	0	0	0.00
2001	south	0	0	0	0	0	0	0.00
2001	south	1	2,434	4,901	3,394	537	11,265	86.66
2001	south	2	64	1,539	244	36	1,883	14.49
2001	south	3	0	24	260	18	302	2.32
2001	south	4	16	0	0	0	16	0.12
2001	south	5	7	0	0	0	7	0.06
2003	north	0	0	0	0	0	0	0.00
2003	north	1	901	201	50	0	1,151	8.86
2003	north	2	231	51	0	0	282	2.17
2003	north	3	11	27	0	0	37	0.29
2003	north	4	885	1,362	30	0	2,276	17.51
2003	north	5	530	0	0	0	530	4.08
2003	south	0	0	0	0	0	0	0.00
2003	south	1	1,358	3,754	582	0	5,694	43.80
2003	south	2	0	35	735	55	825	6.34
2003	south	3	0	0	220	85	305	2.34
2003	south	4	0	0	6	68	74	0.57
2003	south	5	124	0	0	0	124	0.96
2003	south	6	0	0	54	0	54	0.41
2003	south	7	0	0	1	0	1	0.01
2003	south	8	0	0	64	408	472	3.63

[a]Results given for four layers within each patch (0–5 m, 5–13 m, 13–20 m, and 20–30 m) as well as the values integrated over the top 30 m. Note, values >0 in survey 0 of N′01 (prepatch survey) resulted from the bimodal distribution of particulate backscattering values (Figure S3, dashed lines). This meant that the technique for defining the presence of chalk had greater errors (see section 3.4), and positive mass of chalk was estimated when there was none. PIC, particulate inorganic carbon.

described first, followed by a discussion of likely dispersion mechanisms and implications for coccolithophore bloom development.

4.1. Advantages and Limitations of the Chalk-Ex Experimental Design

[53] One advantage of our experimental design was that we knew, with high precision, how much chalk was added to the water. This allowed inverse approaches for calculating chalk mass as well as the determination whether there was sufficient signal to noise to detect the PIC backscattering. Another advantage to the design was that the chalk, being of uniform size, was well-calibrated to backscattering within 3–5% error (on the basis of the standard error of the dilution curves shown in Figure 4a). Moreover, the light-scattering photometers used in this work were calibrated within 0.01–0.07% of each other. Indeed, the calibrations were good enough to detect slight differences between the properties of the 2001 and 2003 chalk batches. Despite the good calibration, it was not clear why the error bars for the field ECO VSF measurements for 2001 (Figure 4b) were larger than those for the 2003 deployment (Figure 4c), since the same instrument was used in both experiments. Finally, the patch was created relatively quickly (~4–5 h) relative to patch evolution on a timescale of several days.

[54] There were also some important limitations to the experimental design that translated to several potential sources of error. The finite duration of patch creation (4–5 h) and subsequent surveys (3–4 h) resulted in errors of order ±0.2 days in estimates of chalk loss rate. The survey patterns themselves (“wagon wheel” or “radiator”) had associated errors. The wagon wheel pattern provided focused sampling at the patch center but increasingly diffuse sampling, moving radially away from the patch center. We used this pattern when we had a good idea where the patch was. The regular sampling of the radiator pattern provided a better chance of finding a small feature far from the supposed patch center, but took longer to complete (about double the time needed for a wagon wheel survey). This lowered the temporal resolution to detect patch evolution, particularly important after initial patch deployment when the chalk concentrations were highest. Errors in krigging of the Scanfish data were low for vertical sections, because of the high frequency with which the Scanfish undulated. However, krigging errors for data between Scanfish sections (i.e., for the plan view maps) were higher (±100%), and if errors exceeded this amount, the data simply were not contoured, which undoubtedly affected the chalk mass balance estimates. Another source of error was that the backscattering properties of each chalk patch were compared to the light-scattering properties of the waters just prior to deployment of the patch. Backscattering heterogeneities within the survey area, or changes in the background backscattering after the prepatch survey, increased the overall variance. This, then, increased the statistical threshold for discriminating chalk backscattering versus all other background backscattering (i.e., it became harder to resolve the chalk). A good example of this was the N′01 area where heterogeneities in backscattering during the prepatch survey resulted in a bimodal distribution of particulate backscattering (Figure S3).

4.2. Criterion for Defining the Border of the Patch

[55] One of the biggest challenges in Chalk-Ex was to define the patch boundary. This was important for optimizing the Scanfish surveys, in order to sample both water

Table 2. Backscattering Statistics for Each Layer and Survey During Chalk-Ex Experiments

Year	Site	Survey	Time (h)	Layer	Particle Backscattering Statistics (530 nm)					Percent > Median +2 Sigma	Percent > Mean +2 Sigma
					Min	Max	Median	Mean	Std Dev		
2001	north	0	−14	1	0.00121	0.00274	0.00143	0.00163	0.00037	12.037	6.713
2001	north	0	−14	2	0.00112	0.00291	0.00139	0.00152	0.00031	11.8925	8.6867
2001	north	0	−14	3	0.00111	0.00354	0.00142	0.00153	0.00032	10.9091	8.7013
2001	north	0	−14	4	0.00083	0.00456	0.00142	0.00152	0.00031	10.3352	8.9385
2001	north	1	3.5	1	0.00107	0.10148	0.00143	0.00330	0.01088	2.1505	2.1505
2001	north	1	3.5	2	0.00124	0.00321	0.00142	0.00144	0.00019	2.3256	2.3256
2001	north	1	3.5	3	0.00099	0.0021	0.00142	0.00143	0.00016	2.7027	2.7027
2001	north	1	3.5	4	0.00125	0.00192	0.00141	0.00142	0.00012	1.7857	1.7857
2001	north	2	10	1	0.00035	0.00621	0.00138	0.00144	0.00039	2.008	2.008
2001	north	2	10	2	0.0011	0.00615	0.00137	0.00139	0.00030	0.86207	0.64655
2001	north	2	10	3	0.00105	0.0019	0.00134	0.00135	9.44E-05	3.9702	3.4739
2001	north	2	10	4	0.00075	0.00873	0.00134	0.00137	0.00034	0.35524	0.35524
2001	north	3	20	1	0.00105	0.00333	0.00133	0.00137	0.00018	3.0853	2.7223
2001	north	3	20	2	0.00056	0.0026	0.00133	0.00134	0.00012	3.0016	2.6856
2001	north	3	20	3	0.00079	0.00263	0.00133	0.00134	0.00010	2.5356	1.6459
2001	north	3	20	4	0.00068	0.00249	0.00133	0.00134	0.00010	2.7727	2.0414
2001	south	0	−6	1	0.00026	0.00625	0.00082	0.00087	0.00034	3.1561	2.99
2001	south	0	−6	2	0.00028	0.00165	0.00082	0.00082	0.00015	2.3718	2.3718
2001	south	0	−6	3	0.00028	0.00146	0.00079	0.00081	0.00014	3.6395	3.4662
2001	south	0	−6	4	0.0001	0.00415	0.00081	0.00081	0.00017	1.365	1.4243
2001	south	1	2.3	1	2.00E-05	0.0118	0.00083	0.00119	0.00148	5.0054	5.0054
2001	south	1	2.3	2	0.00015	0.0114	0.00092	0.00183	0.00222	11.3682	8.9537
2001	south	1	2.3	3	0.00018	0.00925	0.0009	0.00174	0.00198	11.5202	8.4323
2001	south	1	2.3	4	0.00023	0.0085	0.00084	0.00112	0.00107	5.2101	4.958
2001	south	2	24	1	0.0004	0.00432	0.00088	0.00095	0.00030	4.8304	3.0832
2001	south	2	24	2	0.00013	0.00515	0.00089	0.00104	0.00054	5.6246	4.8549
2001	south	2	24	3	0.00035	0.00291	0.00088	0.00092	0.00027	4.3304	3.8641
2001	south	2	24	4	0.00012	0.00351	0.00082	0.00084	0.00021	3.0562	2.9213
2001	south	3	31	1	0.00045	0.00168	0.00087	0.00088	0.00015	4.3988	3.9589
2001	south	3	31	2	0.00029	0.00816	0.00088	0.00090	0.00028	2.1265	1.7993
2001	south	3	31	3	8.00E-05	0.0029	0.0009	0.00095	0.00025	4.2667	4
2001	south	3	31	4	6.00E-05	0.0033	0.00092	0.00093	0.00021	3.1489	3.1489
2001	south	4	48	1	0.00038	0.00656	0.00088	0.00102	0.00050	4.3046	2.9801
2001	south	4	48	2	0.00025	0.0063	0.00079	0.00083	0.00024	1.9939	1.9939
2001	south	4	48	3	0.00025	0.00279	0.00078	0.00080	0.00014	2.3993	2.2279
2001	south	4	48	4	0.00035	0.00337	0.00078	0.00081	0.00016	1.626	1.4384
2001	south	5	78	1	0.00012	0.00507	0.00088	0.00095	0.00044	3.75	3.6111
2001	south	5	78	2	4.00E-05	0.00373	0.00088	0.00088	0.00019	2.3471	2.3471
2001	south	5	78	3	0.0002	0.00279	0.00087	0.00087	0.00015	1.6963	1.9859
2001	south	5	78	4	0.00035	0.00294	0.00083	0.00085	0.00014	2.9199	2.1691
2003	north	0	−9	1	0.00026	0.00754	0.00169	0.00192	0.00077	5.0584	4.1505
2003	north	0	−9	2	0.00025	0.00589	0.00185	0.00189	0.00039	2.9365	2.7763
2003	north	0	−9	3	0.0009	0.00588	0.00197	0.00202	0.00037	4.3582	3.7015
2003	north	0	−9	4	0.00078	0.00876	0.00154	0.00166	0.00058	3.2258	2.6613
2003	north	1	4	1	0.00031	0.01673	0.00214	0.00288	0.00214	8.1448	7.0588
2003	north	1	4	2	0.00027	0.01166	0.0019	0.00214	0.00099	4.5002	4.2406
2003	north	1	4	3	0.00058	0.00649	0.00168	0.00174	0.00045	2.35	2.35
2003	north	1	4	4	0.00039	0.00978	0.00144	0.00147	0.00036	0.9324	0.8991
2003	north	2	12.25	1	0.00042	0.00952	0.00167	0.00207	0.00097	6.5217	4.9872
2003	north	2	12.25	2	0.00027	0.00628	0.00172	0.00187	0.00053	6.6964	5.7478
2003	north	2	12.25	3	0.00021	0.00609	0.00174	0.00182	0.00037	4.0448	3.8581
2003	north	2	12.25	4	0.00016	0.00677	0.00156	0.00158	0.00033	1.4512	1.2753
2003	north	3	24	1	0.00021	0.01398	0.00194	0.00228	0.00118	4.7149	3.7281
2003	north	3	24	2	0.00049	0.01457	0.00175	0.00193	0.00075	3.4682	2.7989
2003	north	3	24	3	0.00036	0.0091	0.001385	0.00143	0.00034	3.2269	2.6718
2003	north	3	24	4	0.00016	0.008	0.00118	0.00119	0.00021	0.9966	0.87506
2003	north	4	30	1	0.00111	0.00923	0.0018	0.00212	0.00105	4.6062	3.789
2003	north	4	30	2	0.0004	0.00979	0.00168	0.00199	0.00089	5.8399	4.239
2003	north	4	30	3	0.00014	0.00732	0.00158	0.00175	0.00055	8.1303	5.7683
2003	north	4	30	4	0.00015	0.00723	0.00136	0.00143	0.00041	4.1812	3.7166
2003	north	5	52	1	0.00012	0.04517	0.00144	0.00250	0.00366	5.303	4.0909
2003	north	5	52	2	3.00E-05	0.01496	0.00144	0.00154	0.00079	1.7922	1.7557
2003	north	5	52	3	0.00038	0.00643	0.0014	0.00143	0.00026	3.7111	3.4318
2003	north	5	52	4	0.00015	0.00739	0.00128	0.00133	0.00029	3.3379	2.4897
2003	south	0	−10	1	0.00027	0.00506	0.00129	0.00131	0.00029	2.8873	2.8169
2003	south	0	−10	2	0.00066	0.00447	0.00128	0.00127	0.00020	0.98668	1.0853
2003	south	0	−10	3	0.00023	0.0023	0.00128	0.00127	0.00012	1.2084	1.5326
2003	south	0	−10	4	0.00044	0.00242	0.0012	0.00120	0.00014	2.3013	2.3013
2003	south	1	3	1	0.00014	0.01161	0.00126	0.00200	0.00182	11.6667	7.7778

Table 2. (continued)

Year	Site	Survey	Time (h)	Layer	Particle Backscattering Statistics (530 nm) Min	Max	Median	Mean	Std Dev	Percent > Median +2 Sigma	Percent > Mean +2 Sigma
2003	south	1	3	2	0.00021	0.01525	0.0013	0.00201	0.00187	9.226	6.5607
2003	south	1	3	3	0.00059	0.01022	0.00127	0.00147	0.00091	4.8164	4.5154
2003	south	1	3	4	0.00042	0.00232	0.00106	0.00108	0.00016	4.1408	3.5611
2003	south	2	10	1	0.00041	0.00935	0.00125	0.00139	0.00064	3.7948	3.4434
2003	south	2	10	2	0.00022	0.01349	0.00128	0.00130	0.00035	1.5944	1.5664
2003	south	2	10	3	0.0004	0.00446	0.00136	0.00143	0.00028	4.7744	3.2701
2003	south	2	10	4	0.00072	0.00623	0.00121	0.00124	0.00024	3.253	2.7849
2003	south	3	23	1	8.00E-05	0.01501	0.00117	0.00128	0.00074	2.1531	2.0335
2003	south	3	23	2	0.00021	0.00419	0.00118	0.00120	0.00021	2.0995	1.9995
2003	south	3	23	3	0.0007	0.00354	0.00129	0.00133	0.00025	4.7318	3.918
2003	south	3	23	4	0.00052	0.00433	0.0012	0.00124	0.00023	4.8404	4.1936
2003	south	4	32	1	0.00059	0.01204	0.00128	0.00146	0.00075	4.0226	3.6455
2003	south	4	32	2	0.00063	0.01224	0.00124	0.00129	0.00040	1.7693	1.7233
2003	south	4	32	3	0.00063	0.002	0.00125	0.00127	0.00014	5.3892	4.5182
2003	south	4	32	4	0.00039	0.00224	0.00124	0.00127	0.00019	5.0237	4.1327
2003	south	5	46	1	0.00019	0.01533	0.0012	0.00156	0.00132	4.2522	3.8123
2003	south	5	46	2	0.00016	0.02096	0.00115	0.00124	0.00064	2.1665	1.9231
2003	south	5	46	3	0.00071	0.00739	0.00121	0.00123	0.00020	2.0923	1.8917
2003	south	5	46	4	0.00033	0.00286	0.0012	0.00121	0.00017	3.1917	3.0087
2003	south	6	58	1	0.0008	0.00963	0.00119	0.00125	0.00038	2.5941	2.3906
2003	south	6	58	2	5.00E-05	0.00516	0.00119	0.00121	0.00018	1.6375	1.5639
2003	south	6	58	3	0.00076	0.00293	0.00133	0.00137	0.00021	5.3433	3.6695
2003	south	6	58	4	0.00023	0.0036	0.00122	0.00125	0.00018	5.5363	4.6764
2003	south	7	69	1	0.00018	0.00801	0.00111	0.00121	0.00053	2.9517	2.6463
2003	south	7	69	2	0.00019	0.00947	0.00111	0.00112	0.00020	1.1947	1.1244
2003	south	7	69	3	0.00078	0.00261	0.00126	0.00129	0.00021	4.5343	3.6356
2003	south	7	69	4	0.00041	0.00255	0.00121	0.00125	0.00019	6.4193	5.23
2003	south	8	79	1	0.00024	0.00745	0.00113	0.00120	0.00049	3.8793	3.5201
2003	south	8	79	2	0.00043	0.0044	0.00114	0.00113	0.00023	2.0848	2.1091
2003	south	8	79	3	0.00049	0.00244	0.00124	0.00127	0.00027	4.0909	3.1534
2003	south	8	79	4	0.00041	0.00289	0.00128	0.00131	0.00025	4.4382	3.6385

inside and outside the patch for comparison. Histograms of backscattering from prepatch waters typically had a quasi-lognormal distribution with the mean and median backscattering values similar but not identical (e.g., Figure 17a; note, there were exceptions to this, such as in N′01 and N′03 patches). Following chalk deployment, histograms became skewed or bimodal (since we sampled both inside and outside the patch; e.g., Figure 5a, area 2), mean backscattering increased relative to the median backscattering, and overall variance increased (Figure 17a; compare prepatch and postpatch error bars). Moreover, the median backscattering value within each layer (at a given site) was more stable than the mean, whether or not chalk had been added to the water (Figure 17b).

[56] We used the prepatch median backscattering plus two standard deviations as the criterion for the presence of chalk. In the few cases when the prepatch survey of backscattering was bimodal (always with one large mode and a secondary subordinate mode) the median better described the major mode than did the population mean. This, combined with the stability of the prepatch medians (Figure 17b), provided the most robust, stable criterion for the presence of chalk. This stability also confirmed that the backscattering properties outside the patch were not changing significantly within a given site during each experiment.

[57] The success of this approach is evident in the reasonable agreement between the northern patch boundaries observed from the aerial photography with the patch boundaries estimated from the krigging of the Scanfish data (Figure 10f). That is, the positions of the Scanfish measurements that produced the krigged boundary (orange line in Figure 10f) were taken along the ship track denoted by red lines (Figure 10f), whereas the aerial photographic images, where available, sampled continuously over the balloon deployment, at meter resolution, to produce the patch boundary (black dashed line). The Scanfish and aerial surveys were separated in time by 3 h. Further circumstantial evidence that the patch border criteria were accurate comes from an examination of the plan views of the patch from each layer. After Lagrangian correction of each Scanfish survey based on the drifters, there was good coherence in the patches observed in the four vertical layers. That is, even though patches were near the limits of detection, the Lagrangian-corrected patches lay on top of each other (Figure 6a, areas 1, 2, and 3; Figure 6b, areas 1, 2, and 3; Figure S5a, areas 1, 2, and 3; Figure S5b, areas 2, 3, and 4; Figure S9a, areas 1 and 2; and Figure S9d, areas 1 and 2).

4.3. An Inverse Approach to Resolving the N′01 Patch Observations

[58] The N'01 patch results represented a special case, since the chalk was essentially undetectable within the timescales of patch deployment and initial survey. The question arises whether, given the strong winds and active mixing, we would have expected the chalk to be undetectable. From the cruise track during the 7.5-h chalk deployment, the patch began with a roughly circular shape, with diameter of ~800 m (Figure 3a). Evenly distributed over the observed mixed layer depth of 60 m, the 13,000 kg of chalk should have had a final concentration of 0.0043 mol

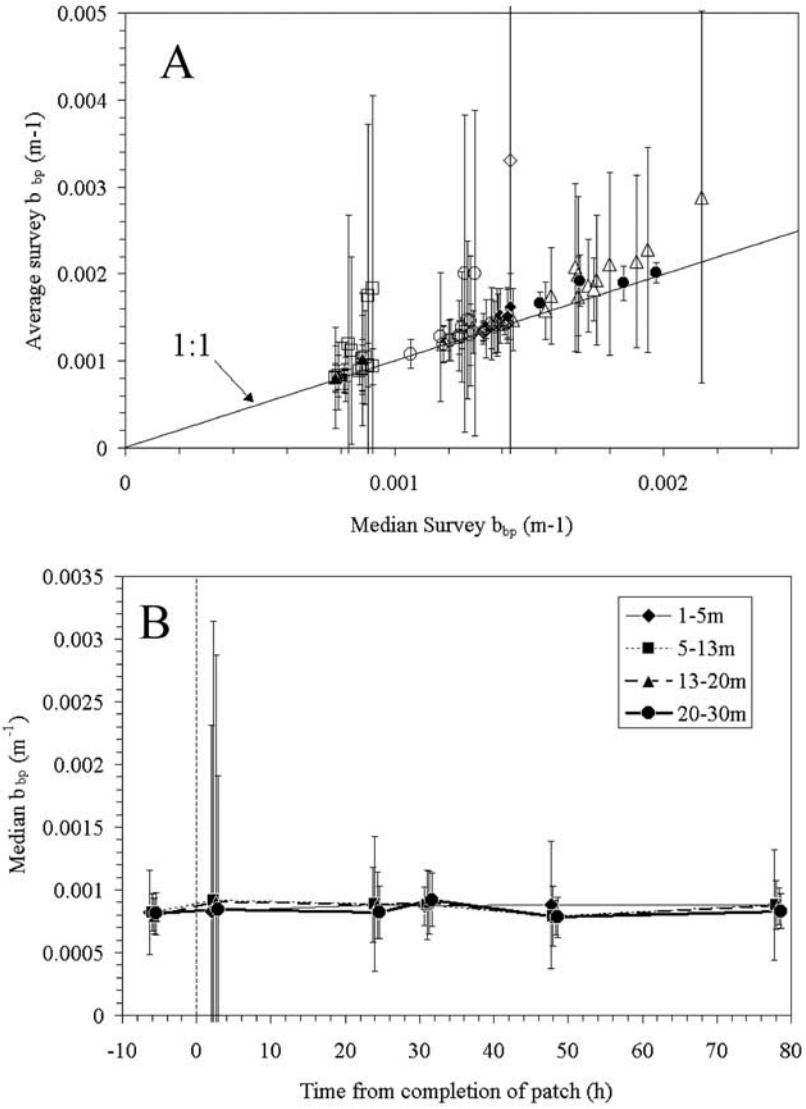

Figure 17. (a) Mean b_{bp} plotted against median b_{bp} from the same survey for each of the four layers. Error bars represent standard deviation about the mean b_{bp}. Solid symbols represent prepatch Scanfish survey results, while open symbols represent postpatch survey results. Symbols represent four patches: diamonds, N′01; squares, S′01; triangles, N′03; and circles, S′03. The 1:1 line is shown for reference. One can see that prepatch medians and means typically were within 0.0002 m^{-1} of each other, while postpatch means exceeded the median values by 0.001–0.002 m^{-1}. The largest disparities were from the first postpatch Scanfish surveys. (b) Time course of the median particulate backscattering for S′01 patch within each layer: diamonds, 1–5 m; squares, 5–13 m; triangles, 13–20 m; and circles, 20–30 m. Error bars represent the standard deviation from the mean. Zero time represents the termination of chalk deployment. Note stability of median b_{bp}, whether or not chalk was deployed.

PIC m^{-3}, and, using the calibration equations from Figure 4a, particle backscattering of 0.005 m^{-1} would have been detected. This would have been easily detectable using the ECO VSF provided that it was contained within the confines of the 800-m diameter circular area.

[59] So, why did we not detect chalk? The median b_{bp} at 530 nm in the N'01 prepatch survey, over the four layers, was $\sim 1.41 \times 10^{-3}$ m^{-1}, barely lower than the mean value (1.56×10^{-3} m^{-1}), and the variance was $\pm 0.34 \times 10^{-3}$ (for a coefficient of variation of 21.6%). Using the median plus twice the standard deviation as the criterion for chalk detection (2.1×10^{-3} m^{-1}) translates to a threshold concentration of 1.79×10^{-3} mol m^{-3} (Figure 4a). This concentration would have been achieved in a circular patch if the diameter of the patch had increased to 1.2-km diameter (with the 60-m mixed layer) soon after deployment. Three factors argue for this to be the case: (1) unlike other deployments where previously deployed chalk could be used as a navigational aid, visual clues were limited for the N′01 patch; this resulted in a larger, less concentrated patch (Figure 3a) for which the 800-m diameter based on the final loop is likely an underestimate, (2) the N′01 patch took the longest to deploy (>7 h versus 4–5 h for the others), and (3) size estimates from the other patches (Figure 16),

deployed under more quiescent wind conditions, indicate that diameters of 2 km were reached within 2–5 h. Thus, it is likely that the N′01 patch had a diameter exceeding 1.2 km by the time of the first CTD cast (2 h after the end of chalk deployment, 9 h from the start of deployment), making the chalk undetectable. The beam attenuation levels 9 h after deployment were slightly less than in the prepatch profiles, down to 100-m depth (Figure 9f).

4.4. Vertical Descent of the Chalk

[60] It was clear from all patch deployments that between surveys the chalk was being mixed vertically, subducted, or both. On the basis of the plan view layer surveys, the chalk was seen to descend through the four layers. For example, for survey 1 of S′03, the chalk was mostly between 1 and 13 m (layers 1 and 2; Figure S5a, areas 1 and 2). By survey 2, 7.5 h later, most of the chalk was between 13 and 20 m (Figure S5b, area 3). A representative vertical descent rate for the chalk descending from layer 1 (1–5 m, average depth = 3 m) to layer 3 (13–20 m, average depth = 16.5 m) between surveys is ~1.8 m h^{-1} (0.05 cm s^{-1}). For descent from layer 2 (5–13 m; average 9 m) to layer 3 (13–20 m, average depth = 16.5 m), the representative rate is ~1.0 m h^{-1} (0.028 cm s^{-1}). Similar descent rates were observed for the S'01 patch. For the N'03 patch, most of the chalk in survey 1 was between 1 and 5 m, and it disappeared by survey 2 (all layers) for a maximum descent rate of 30 m in 7 h or ~4.3 m h^{-1}(0.12 cm s^{-1}). Some of the vertical sections of chalk show little density structure (e.g., Figure 7b); thus we cannot eliminate vertical mixing as a means to move the chalk particles downward, especially early in the deployment. Indeed, previous observations using Lagrangian floats [*D'Asaro et al.*, 1996; *McNeil and Farmer*, 1995] have demonstrated vertical mixing velocities within surface mixed layers as high as 1 cm s^{-1}. The vertical descent velocities observed here were all less than this value, suggesting that vertical mixing was a feasible mechanism for rapid downward transport of chalk after deployment.

[61] The above descent rates were much too fast to be from particle sinking alone given that the sinking rate of 2-μm solitary coccoliths is ~0.14 m d^{-1} (=0.004 m h^{-1}) [*Honjo*, 1976]. *Balch et al.* [1996c] independently verified Honjo's sinking rate using a simple theoretical Stokes formulation to estimate coccolith sinking on the basis of coccolith shape and size. They concluded that subsurface peaks of coccoliths in the North Atlantic, following a large mesoscale bloom of *Emiliania huxleyi*, could only have occurred through in situ calcification and/or vertical subduction of the coccoliths from surface waters, not sinking. Since the chalk used here was obviously inanimate, then the most likely mechanism for its appearance at depth was not sinking but initial vertical mixing then subduction. If the mixed layer shallowed after chalk deployment (e.g., S'01; compare density profiles in Figures 9b and 9c at 15 m), then any chalk mixed vertically downward could have been entrained within the shoaling pycnocline, such as was postulated to occur in the "mixed layer pump" hypothesis [*Gardner et al.*, 1995, 1999]. Internal waves were also evident in the patch cross sections (e.g., Figures 13, S6f, and S6g), providing a mechanism for changes in pycnocline depth independent of local surface forcing. Internal wave excursions, coupled with vertical mixing and horizontal shear, provide another mechanism for entrainment of particles at the mixed layer base and subsequent horizontal spreading (via shear dispersion).

[62] The total mass of chalk in all layers can be compared to the 13,000-kg initial mass to examine the mass balance. The S′01 survey provided the best closure. The first Scanfish survey accounted for 86% of the chalk deployed (Table 1). By the second survey, only 14.5% was found. The percentage of chalk mass accounted for in the other patches was lower still. Thus, without being able to account for all of the chalk, we cannot eliminate the hypothesis that processes other than vertical subduction were responsible for chalk removal from the patch survey area.

[63] Another possible mechanism for rapid removal of chalk was that the dense slurry deployed from the ship rapidly sank as a cohesive water parcel to depths below the maximum Scanfish survey depth (30 m) before the first measurements were made. This was unlikely for several reasons. First, the initial chalk slurry (0.528 kg of chalk L^{-1} or 5280 mol m^{-3}), while dense, was dispersed through 4-mm holes along the spreader on the ship's transom into the ship's propeller wash. The streams visibly dissipated as the ship steamed forward at about 50 cm s^{-1}. One can use standard wake dispersal calculations to predict the initial wake concentration of chalk. The ship's draft (D) was 5.6 m, and beam (B) was 10.1 m. The wake cross-sectional area within which the chalk would have initially mixed is calculated according to *Csanady* [1978] as $8 \times B \times D$ (or 454 m^2). At a speed of 1.8 km h^{-1} (V_s), slurry concentration (C_i = 5.28 M), and slurry pumping rate (Q) of 98 L min^{-1}, the initial wake concentration of chalk was equal to $(Q \times C_i \times 60 \times 0.001)/(V_s \times S \times 1000)$ = 38.06 μM (=3.805 $\times$ 10^{-2} mol m^{-3}) [*Coale et al.*, 1998; *Csanady*, 1978]. Using the average of the two calibrations in Figure 4, the predicted chalk backscattering in the wake would have been ~0.05 m^{-1}.

[64] The maximum observed b_{bp} during the first Scanfish surveys following chalk deployment was ~0.015 m^{-1}, less than expected from the wake dispersal calculations (Table 2; note, in N′01 in the aborted Scanfish survey the maximum b_{bp} was 0.10 m^{-1}) suggesting the above wake dispersal calculations were conservative (0.05 m^{-1} predicted versus 0.015 m^{-1} observed). However, using above-water radiance measurements of the patch, the maximum b_{bp} value was 0.041 m^{-1} (seen in N'03; Figure 11), closer to the 0.05 m^{-1} b_{bp} predicted from the wake dispersion calculations. Thus, both wake dispersion estimates and surface observations argue for a maximum density anomaly of the chalk immediately after deployment of 2.85×10^{-3} kg m^{-3} which is only ~2.8×10^{-4} % of the typical seawater density in the upper 30 m. Thus the chalk-induced density change was negligible.

[65] A second reason that we believe that the chalk remained in the surface layer, rather than sinking rapidly out before we could sample it with the Scanfish, was that CTD casts to 60–100-m depth were done as little as ~1 h after each patch was deployed. The CTD beam transmissometer data (Figure 9) demonstrated that the PIC was in the top 15 m initially, just as the Scanfish data showed, and there was no evidence of any anomalously high beam attenuance deeper in the water column. Last, the fact that little chalk was caught in the floating sediment traps (C. H. Pilskaln et al., submitted manuscript, 2009) (suspended at 60 m during the 2001

deployments (below layer 4) and 15–16 m in the 2003 deployments (below layers one and two and part of layer 3)) suggests that sinking was not important to the optical evolution of the patch. Aggregation of the chalk was not observed in shipboard experiments, either, eliminating another means to increase vertical sinking rates of the chalk (C. H. Pilskaln et al., submitted manuscript, 2009).

[66] Small-scale physical processes clearly did affect the patch distribution. Heterogeneities on the order of tens of meters were evident in the chalk distribution based on the aerial images from S′01 and S′03 patches (Figure 10). This suggested the possible influence of Langmuir circulation in the surface layer [*Colbo and Li*, 1999; *Scott et al.*, 1969]. However, CTD profiles from the first postpatch surveys of S′01 and S′03 demonstrated that strong pycnoclines initially would have restricted Langmuir cells to the top 15 m. Furthermore, vertical profiles of density in S'01 showed that the mixed layer became ''capped'' with lighter water, which would have inhibited Langmuir cell growth (Figures 9a–9d). Thus, while mixing processes driven by surface forcing presumably redistributed chalk both horizontally and vertically, they did not likely result in redistribution of the chalk below 30 m for S′01 and S′03.

4.5. Eddy Diffusion, Horizontal Gradients, and Chalk Dispersal

[67] Turbulent eddy diffusion (both horizontal and vertical) is a likely factor affecting the mixing and dispersion of the chalk patches. The stages of mixing of water masses was elegantly described in a classic paper by *Eckart* [1948]: when two water masses begin as distinct patches, subsequent stirring initially distorts and steepens the gradients (intermediate stage), after which the gradients gradually disappear and the liquid becomes homogeneous (final stage). *Stommel* [1949] showed the limitations of the Fickian diffusion equation for describing horizontal eddy diffusion in the sea. Instead, he promoted the Richardson law [*Richardson*, 1926] of diffusion [see also *Kolmogorov*, 1941], consistent with the observation that the diffusivity increased as the mutual separation of the water parcels to the 4/3 power [*Stommel*, 1949]. Stommel's aircraft observations of floating drifters provided strong evidence on horizontal eddy diffusion and its dependence on size scale.

[68] Biological particle gradients in the sea, in the face of significant turbulent diffusion, can only be maintained by equally rapid particle production rates such as exponential growth of organisms [*Okubo*, 1978]. In Chalk-Ex, the production was rapid, taking place in 0.2 days, and the time evolution of patch area was the same for S′01, N′03, and S′03 patches; that is, patch area increased from initial patch deployment to the first Scanfish survey, then held steady or decreased thereafter (Figures 16b, 16c, and 16d). We believe that the decrease in size was an artifact of sampling limitations, resulting from the dilution of the chalk at the patch periphery to concentrations below the statistical threshold for detection. Our experimental design would have benefited from the use of sulphur hexafluoride (SF-6) as a tracer of the patch as by *Stanton et al.* [1998] since it can be detected at extremely low concentrations and provides a true Lagrangian tracer with which to compare to the distributions of chalk particles over space and time. Unfortunately, this was not possible within the constraints of our experiment.

[69] The rate of increase in patch area between the time of chalk deployment (where the ship's navigation provided a highly accurate estimate of patch size) and the first Scanfish survey (when chalk concentrations were still high enough to accurately define the patch dimensions) provided the most accurate estimate of horizontal eddy diffusivity at our patch sites (Figures 16b, 16c, and 16d). On the basis of S′01, N′03 and S′03 results, estimates of horizontal eddy diffusion were 519, 108, and 747 $m^2\ s^{-1}$, respectively. These values compare favorably to eddy diffusivity estimates made in the same fashion (but using SF-6) during Iron-Ex-I in the equatorial Pacific. In those experiments, mean horizontal eddy diffusivities were $600 \pm 100\ m^2\ s^{-1}$ along the axis of the wind and $200 \pm 30\ m^2\ s^{-1}$ orthogonal to the wind [*Stanton et al.*, 1998].

[70] Our diffusivity estimates should be interpreted cautiously, however, since the fraction of the original chalk that was accounted for in the first Scanfish surveys of S′01, N′03, and S′03 was 86.7%, 8.9%, and 43.8% respectively. One can partially correct for the unaccounted chalk by dividing the area of the patch by the fraction of the original chalk mass that was found. (This implicitly assumes that chalk was present just outside the patch boundaries at concentrations infinitesimally below the limit of detection). Applying such a correction globally over our Scanfish surveys gave higher average horizontal eddy diffusivities of 542, 1210, and 2546 $m^2\ s^{-1}$ for the S′01, N′03, and S′03 patches, respectively (Figure 16e). If the chalk outside the patch diffused to lower concentrations than assumed by the 2-sigma cutoff (highly likely), then for conservation of mass, the patch would have had to be proportionally larger (meaning that the eddy diffusion also would have been even greater than our estimates here).

4.6. Formation of Thin Layers of Chalk

[71] Particle distributions in the surface ocean reveal much about the processes that control their distributions. Indeed, particle maxima are typically found in the surface waters of the world ocean. Subsurface maxima of phytoplankton were described in the classic model of *Riley et al.* [1949], as well as a number of other works [*Lorenzen*, 1966, 1967; *Steele and Yentsch*, 1960; *Strickland*, 1968]. Numerous hypotheses exist to explain what controls the formation of subsurface maxima of chlorophyll, biomass and particle abundance. Physical mechanisms have been hypothesized to concentrate particles at frontal boundaries [*Cullen and Eppley*, 1981; *Cullen et al.*, 1982; *Karabashev and Solov'yev*, 1978; *Pingree*, 1978; *Pingree et al.*, 1975]. More recently, near-inertial wave shear has been suggested as a means to form thin layers of particles that are tens of centimeters thick [*Franks*, 1995], where the thickness is a function of the vertical shear rates and the along-isopycnal length of the phytoplankton patches. Biological mechanisms have also been hypothesized for formation of subsurface maxima. For example, one hypothesis is that subsurface particle maxima represent optimal growth zones for phytoplankton, with sufficient light (propagating downward from above) and sufficient nutrients (diffusing upward from below) [*Cullen et al.*, 1982; *Holligan et al.*, 1984]. Another biological hypothesis invokes differential grazing pressure above and below, but evidence for this is minimal [*Cullen*, 1982; *Cullen and Eppley*, 1981]. More recently, thin layers have

been described that are between 0.5- and 5-m thick and persist for timescales of days [*McManus et al.*, 2003; *Rines et al.*, 2002].

[72] In Chalk-Ex, we observed that the chalk became capped by lower density water as a result of surface heating and horizontal advection/intrusion events, and that the chalk was subsequently subducted along density surfaces while the patch was elongated. The prototypical case for this process is the S′01 patch, although S′03 and N′03 also show evidence of this phenomenon The presence of several-meters-thick, high-backscattering layers along density surfaces (Figures 8b, 8c, 8d, 13e, 13f, 15g, S2b, S2c, S6f, S6g, and S7g) was unequivocal, however.

[73] The fact that the chalk particles were inanimate eliminates most biological mechanisms for thin layer formation (including the grazing hypothesis since rates of chalk grazing were shown to be insignificant (C. H. Pilskaln et al., submitted manuscript, 2009)). Thus, the question is which of the physical mechanisms (or combinations thereof) are the most likely for forming the thin layers. We believe that a combination of subduction, sinking, and shear dispersion was responsible for formation of the thin layers. Of the three processes, sinking appeared to be the least important factor, given the small sinking rates of isolated chalk particles, the lack of evidence for particle aggregation, and the fact that chalk patches were typically distributed along, rather than across, isopycnals. The exception to this was the initial stages of S′03 patch evolution, where the patch was distributed across a density gradient of 0.02 kg m^{-3} within the upper 15 m (Figure 12) prior to being found along isopycnal surfaces at a density higher than the density of the injection region (Figure 13). Still, sinking of individual 2-μm chalk particles (0.1 m d^{-1}) would have been too slow to move the particles to 20–30-m depths where they were ultimately found on a timescale of a day. Thus, the inference is that chalk particles were subducted to the base of the mixed layer at rates of 1–4 m h^{-1} where they encountered the pycnocline and became concentrated because of the greatly increased density gradient. Shear dispersion processes would act to mix the chalk laterally both during and after the subduction process. This is consistent with the observed elongation of the patch along the upper pycnocline (Figures 8, 13, 15, and S6). This combined mechanism is compatible with the observations of *Osborn* [1998].

4.7. Insights for Coccolithophore Bloom Development

[74] The results of Chalk-Ex provide insights into the maintenance and development of coccolithophore blooms. In four patch experiments, each with varying mixed layer dynamics, a kilometer-sized patch became undetectable in 1–2 days, or, in the case of the N′01 patch, it became undetectable within 2 h after chalk deployment was completed. Overall, the rate that chalk became undetectable was extraordinarily fast, with specific rates between 2 and 4 d^{-1}. Coccolithophore blooms observed from space-based remote sensing are 2–3 orders of magnitude larger than the patches that we produced in Chalk-Ex, and typically, these high-reflectance waters are detectable for 2–3 weeks. [*Balch*, 2004; *Balch et al.*, 2005, 1991; *Brown and Yoder*, 1994; *Holligan et al.*, 1993, 1983; *Tyrrell and Merico*, 2004].

[75] Critical patch size is defined as the minimal horizontal scale below which no increase in abundance is possible because of dispersive effects of turbulence. This was first described over 50 years ago [*Kierstead and Slobodkin*, 1953; *Okubo*, 1978; *Skellam*, 1951]. Critical patch size can be approximated as a "critical radius," R_c, of a two-dimensional circular patch, as a function of horizontal eddy diffusivity, D, and α, the net growth rate of the phytoplankton [*Okubo*, 1978]:

$$R_c = 2.4048(D/\alpha)^{1/2} \quad (1)$$

Okubo [1978] showed that with various models for scaling turbulence and algal growth, R_c would be ~1–2 km for phytoplankton with a net growth rate of 1 d^{-1}, at eddy diffusivity levels of about 8 m^2 s^{-1}, well below the turbulence levels that we estimated on the basis of the rate of change of the area of the chalk patches.

[76] In chemostat cultures of *Emiliania huxleyi*, the coccolith detachment rate is equivalent to the coccolithophore growth rate [*Fritz*, 1999; *Fritz and Balch*, 1996]. Thus, for a coccolithophore patch to remain visible as a high-reflectance feature, losses due to turbulence and mortality must be minimal [*Tyrrell and Merico*, 2004] and growth rates (and coccolith production rates) must remain high to offset these losses. Indeed, in the Gulf of Maine, a frequent site of coccolithophore blooms, such blooms are virtually always observed near the summer solstice (as water columns are becoming strongly stratified) [*Balch*, 2004]. Moreover, they begin in the stratified waters on the eastern side of Jordan Basin, on the stratified side of the Scotian front. Thereafter, the blooms spread into the middle of the Jordan Basin as the surface waters stratify further [*Balch*, 2004]. The smallest persistent blooms that we have observed in a 9-year time series in the Gulf of Maine have been ~30-km-wide [*Balch et al.*, 2008]. Assuming (1) this minimum bloom size was the critical patch size and (2) a realistic net growth rate (and detachment rate) for field *E. huxleyi* is 0.5 d^{-1} [*Balch et al.*, 1996a], then the horizontal eddy diffusivity necessary to constrain such a patch would have been ~900 m^2 s^{-1}, about half the diffusivity that we estimated in our N′03 patch in Jordan Basin (during June). In other words, crude diffusivity estimates based on the smallest coccolithophore blooms seen in the Gulf of Maine (and their approximate growth rates) are within a factor of two of turbulence estimates that we made during Chalk-Ex.

5. Summary and Conclusions

[77] We successfully generated several coherent, kilometer-sized chalk patches using techniques similar to those employed in earlier Iron-Ex experiments [*Coale et al.*, 1998]. We used a statistical approach to optically detect the patch over spatial scales of 10 km and timescales of several days. The primary limitations of the experimental design were (1) the limit of detection of the chalk as the patch diffused (mostly horizontally) and (2) the survey patterns used by the single ship to spatially resolve the patches through time. The geophysical statistical approach of "krigging" was highly effective for resolving the vertical distribution of the optically active particles over the top 30 m of the water column. Krigging errors were larger, however,

when the survey sections were analyzed over the >10-km-diameter survey areas to produce plan views of the patch.

[78] We were not able to account for 100% of the mass of the chalk in any of the postpatch Scanfish surveys (the most accounted for was 86%). This was because of the rapidity with which the patch dispersed. The rate of dispersal was mainly a function of the level of wind forcing, subduction of the patch along density surfaces, and the strength of density stratification below the mixed layer. Moreover, the rapid loss of chalk could not be attributed to aggregation, rapid sinking, grazing, or dissolution (see companion paper by C. H. Pilskaln et al. (submitted manuscript, 2009)). Specifically, the hypothesis of rapid chalk sinking below the maximum depth of the observations was negated by a number of lines of evidence, all internally consistent with our observations.

[79] Subduction, gradual sinking, and shear dispersion provide the most likely mechanisms for the rapid chalk dispersal; patch observations based on different optical techniques (e.g., in-water measurements of inherent optical properties, above-water radiometry, or high-altitude imagery) were internally consistent. Patch size calculations made early in each deployment provided the best estimates of horizontal eddy diffusivity, and the results were consistent with this physical mechanism of dispersal. Moreover, diffusivity estimates were consistent with calculations made by others (using the same approach). Vertical sections through the patches showed clear evidence for the chalk patch being subducted along isopycnals while being elongated, and then being further sheared into thin layers at the base of the mixed layer. Interestingly, formation of these thin layers occurred without biological processes of growth or mortality (since the chalk particles were inanimate) and without grazing by zooplankton (C. H. Pilskaln et al., submitted manuscript, 2009). This, again, is supportive of a physical dispersal mechanism, applicable to the more general problem of formation of subsurface particle maxima in the sea (such as chlorophyll maxima, thin layers, and nepheloid layers).

[80] Taken together with previous observations of coccolithophore blooms, these observations highlight the importance of rapid coccolith production and detachment for maintenance of a coccolithophore bloom over timescales of several weeks. On the basis of previous work, the minimum size of coccolithophore blooms in the Gulf of Maine (30 km) is fully consistent with the eddy diffusivity values calculated in Chalk-Ex, as applied to the well-known critical patch size concept [*Okubo*, 1978].

[81] Finally, these observations illustrate the importance of the spatial scale for the maintenance of optical gradients in the sea. The optical signature for kilometer-sized surface patches of inanimate particles (such as sediments) will be short-lived in coastal and shelf waters because of horizontal eddy diffusion. It was pointed out previously that for dissipation rates of 10^{-2} s^{-1}, rotating on a horizontal plane at typical inertial frequency, particles that are initially 10 m apart vertically would be predicted to be 1 km apart in just 3 h [*Itsweire and Osborn*, 1988; *Itsweire et al.*, 1989], consistent with our observations. Exponential growth of phytoplankton and bacteria, or exponential release of coccoliths associated with exponential growth of coccolithophores, is the most likely reason that optical gradients in coastal waters are maintained for periods exceeding a few days. Using the critical patch concept, the size of any bio-optical phenomena must exceed the critical patch size, R_c, if the optical gradient is to be stable through time. For satellite remote sensing from Sun-synchronous polar orbiters, the minimum sample frequency is about one sample per day. Our ability to interpret bio-optical changes in terms of growth and mortality will be compromised for features smaller than R_c, since physical processes such as shear dispersion will disperse the small features between consecutive daily satellite overpasses. Natural mortality from grazing will make such features disappear even faster.

[82] There is a continuum of growth rates in the sea, with the smaller organisms typically capable of faster division rates under optimal growth conditions [*Sheldon et al.*, 1972]. Thus, R_c for fast dividing bacteria will be smaller than R_c for slow growing phytoplankton. This has important ramifications for remote sensing. Remote-sensing reflectance (water-leaving radiance just above the sea surface normalized to incident downwelling irradiance [*Mobley*, 1994]) is a function of both spectral backscattering (b_b) and absorption (a), proportional to b_b/a [*Gordon et al.*, 1988]. Absorption of visible light is primarily done by phytoplankton [*Gordon and Morel*, 1983; *Yentsch*, 1962], which have relatively slow growth rates, hence their R_c will be proportionally larger than faster growing bacteria. However, most of the backscattering of visible light is attributed to 1-μm-sized particles, which includes both picoautotrophs as well as heterotrophic bacteria [*Morel and Ahn*, 1990, 1991]. Higher growth rates of the small cells would mean that their critical patch size would be proportionally smaller than for large phytoplankton, meaning that they (and their associated backscattering) are less subject to losses from eddy diffusion. Thus, gradients in phytoplankton absorption would be less stable between daily satellite overpasses than gradients in bacterial backscattering. Put another way, daily, small-scale changes in R_{rs} would more likely result from the eddy diffusion overwhelming the growth of slow growing (light-absorbing) phytoplankton than the fast growing (light-scattering) bacteria. This is why ocean color satellite remote sensing, based on Sun-synchronous, polar-orbiting satellites (with one good overpass per day), will better detect the impact of physics on phytoplankton distributions rather than on bacterial distributions. Conversely, inference of phytoplankton growth from small-scale (<10 km) changes in R_{rs} should be done cautiously, since daily changes more likely result from ocean physics than biological growth and mortality. With the advent of high-resolution ocean color observations from geostationary satellite, it will be possible to better separate physical from biological influences on ocean optical properties, at smaller timescales and space scales. The results will be relevant to both slow growing, absorbing phytoplankton as well as fast growing, backscattering microbes.

[83] **Acknowledgments.** We thank the captains, crew, and shore support staff of the R/V *Endeavor* for their assistance on the 2001 and 2003 cruises. We would like to acknowledge the other investigators in this project for help during all phases of this work, including experimental design, execution, and data interpretation: H. Dam (University of Connecticut), G. McManus (University of Connecticut), C. Pilskaln (University of Massachusetts, Dartmouth), and J. Goes (Bigelow Laboratory). E. Booth (Bigelow Laboratory), N. Galbraith (WHOI), J. Lord (WHOI), M. Lettau (University of New England), B. Thompson (Bigelow Laboratory), L. Mangum (University of Maine, Orono), and A. Smith (University of

Connecticut) provided assistance at sea. The University of Rhode Island shipboard technical support staff (D. Nelson, L. Butler, B. Kidd, and S. Oleano) provided excellent support during both cruises. W. Gardner and an anonymous reviewer provided careful, constructive reviews of an earlier version of the manuscript. We would like to thank the Office of Naval Research/Optical and Biological Oceanography Program for their support of Chalk-Ex with awards N000140110042 (WMB) and N00014-01-1-0141 (AJP). Additional funding for this work came from ONR (N00014-05-1-0111) and NASA (NNG04Gl11G, NNX08AC27G, NNG04HZ25C) to W.M.B.

References

Alldredge, A. L., and M. W. Silver (1988), Characteristics and dynamics and significance of marine snow, *Prog. Oceanogr.*, *20*, 41–82, doi:10.1016/0079-6611(88)90053-5.

Armstrong, R. A., C. Lee, J. I. Hedges, S. Honjo, and S. G. Wakeham (2002), A new, mechanistic model for organic carbon fluxes in the ocean based on the quantitative association of POC with ballast minerals, *Deep Sea Res., Part II*, *49*, 219–236, doi:10.1016/S0967-0645(01)00101-1.

Balch, W. M. (2004), Re-evaluation of the physiological ecology of coccolithophores, in *Coccolithophores: From Molecular Processes to Global Impact*, edited by H. R. Thierstein and J. R. Young, pp. 165–190, Springer, New York.

Balch, W. M., and D. T. Drapeau (2004), Backscattering by Coccolithophorids and coccoliths: Sample preparation, measurement and analysis protocols, in *Ocean Optics Protocols for Satellite Ocean Color Sensor Validation. Revision 5: Biogeochemical and Biological-Optical Measurements and Data Analysis Protocols*, edited by J. L. Mueller, G. S. Fargion, and C. R. McClain, pp. 27–36, NASA Goddard Space Flight Space Cent., Greenbelt, Md.

Balch, W. M., P. M. Holligan, S. G. Ackleson, and K. J. Voss (1991), Biological and optical properties of mesoscale coccolithophore blooms in the Gulf of Maine, *Limnol. Oceanogr.*, *36*, 629–643.

Balch, W. M., J. Fritz, and E. Fernández (1996a), Decoupling of calcification and photosynthesis in the coccolithophere *Emiliania huxleyi* under steady-state light limited growth, *Mar. Ecol. Prog. Ser.*, *142*, 87–97, doi:10.3354/meps142087.

Balch, W. M., K. Kilpatrick, P. M. Holligan, D. Harbour, and E. Fernández (1996b), The 1991 coccolithophore bloom in the central North Atlantic. II. Relating optics to coccolith concentration, *Limnol. Oceanogr.*, *41*, 1684–1696.

Balch, W. M., K. A. Kilpatrick, P. M. Holligan, and C. Trees (1996c), The 1991 coccolithophore bloom in the central North Atlantic. I. Optical properties and factors affecting their distribution, *Limnol. Oceanogr.*, *41*, 1669–1683.

Balch, W. M., D. T. Drapeau, T. L. Cucci, R. D. Vaillancourt, K. A. Kilpatrick, and J. J. Fritz (1999), Optical backscattering by calcifying algae: Separating the contribution by particulate inorganic and organic carbon fractions, *J. Geophys. Res.*, *104*, 1541–1558, doi:10.1029/1998JC900035.

Balch, W. M., D. T. Drapeau, B. C. Bowler, E. S. Booth, J. I. Goes, A. Ashe, and J. M. Frye (2004), A multi-year record of hydrographic and bio-optical properties in the Gulf of Maine: I. Spatial and temporal variability, *Prog. Oceanogr.*, *63*, 57–98, doi:10.1016/j.pocean.2004.09.003.

Balch, W. M., H. R. Gordon, B. C. Bowler, D. T. Drapeau, and E. S. Booth (2005), Calcium carbonate budgets in the surface global ocean based on MODIS data, *J. Geophys. Res.*, *110*, C07001, doi:10.1029/2004JC002560.

Balch, W. M., D. T. Drapeau, B. C. Bowler, E. S. Booth, L. A. Windecker, and A. Ashe (2008), Space-time variability of carbon standing stocks and fixation rates in the Gulf of Maine, along the GNATS transect between Portland, ME and Yarmouth, NS, *J. Plankton Res.*, *30*(2), 119–139, doi:10.1093/plankt/fbm097.

Banse, K. (1994), Grazing and zooplankton production as key controls of phytoplankton production in the open ocean, *Oceanography*, *7*(1), 17–20.

Broecker, W. S., A. Sanyal, and T. Takahashi (2000), The origin of Bahamian whitings revisited, *Geophys. Res. Lett.*, *27*(22), 3759–3760, doi:10.1029/2000GL011872.

Brown, C. W., and J. A. Yoder (1994), Coccolithophorid blooms in the global ocean, *J. Geophys. Res.*, *99*(C4), 7467–7482, doi:10.1029/93JC02156.

Brown, O., and H. Gordon (1974), Size-refractive index distribution of clear coastal water particulates from light scattering, *Appl. Opt.*, *13*, 2874–2881, doi:10.1364/AO.13.002874.

Campbell, J. W. (1995), The lognormal distribution as a model for bio-optical variability in the sea, *J. Geophys. Res.*, *100*(C7), 13,237–13,254, doi:10.1029/95JC00458.

Chin, W. C., M. V. Orellana, and P. Verdugo (1998), Spontaneous assembly of marine dissolved organic matter into polymer gels, *Nature*, *391*, 568–572, doi:10.1038/35345.

Coale, K. H., K. S. Johnson, S. E. Fitzwater, S. P. G. Blain, T. P. Stanton, and T. L. Coley (1998), IronEx-I, an in situ iron-enrichment experiment: Experimental design, implementation and results, *Deep Sea Res., Part II*, *45*, 919–945, doi:10.1016/S0967-0645(98)00019-8.

Colbo, K., and M. Li (1999), Parameterizing particle dispersion in Langmuir circulation, *J. Geophys. Res.*, *104*(C11), 26,059–26,068, doi:10.1029/1999JC900190.

Csanady, G. T. (1978), An analysis of dumpsite diffusion experiments, in *Ocean Dumping of Industrial Wastes*, edited by B. H. Ketchum, D. R. Kester, and P. K. D. Park, pp. 109–129, Plenum Press, New York.

Cullen, J. J. (1982), The deep chlorophyll maximum: Comparing vertical profiles of chlorophyll *a*, *Can. J. Fish. Aquat. Sci.*, *39*, 791–803, doi:10.1139/f82-108.

Cullen, J. J., and R. W. Eppley (1981), Chlorophyll maximum layers of the southern California Bight and possible mechanisms of their formulation and maintenance, *Oceanol. Acta*, *4*(1), 23–32.

Cullen, J. J., F. M. H. Reid, and E. Stewart (1982), Phytoplankton in the surface and chlorophyll maximum off southern California in August, 1978, *J. Plankton Res.*, *4*(3), 665–694, doi:10.1093/plankt/4.3.665.

D'Asaro, E. A., D. M. Farmer, J. T. Osse, and G. T. Dairiki (1996), A Lagrangian float, *J. Atmos. Oceanic Technol.*, *13*(6), 1230–1246, doi:10.1175/1520-0426(1996)013<1230:ALF>2.0.CO;2.

Deutsch, C. V., and A. G. Journel (1992), *GSLIB: Geostatistical Software Library and User's Guide*, 340 pp., Oxford Univ. Press, Oxford, U. K.

Dugdale, R. C., and F. P. Wilkerson (1989), New production in the upwelling center at Point Conception, California: Temporal and spatial patterns, *Deep Sea Res.*, *36*(7), 985–1007, doi:10.1016/0198-0149(89)90074-5.

Eckart, C. (1948), An analysis of the stirring and mixing processes in incompressible fluids, *J. Mar. Res.*, *7*(3), 265–275.

Fernández, E., P. Boyd, P. M. Holligan, and D. S. Harbour (1993), Production of organic and inorganic carbon within a large scale coccolithophore bloom in the northeast Atlantic Ocean, *Mar. Ecol. Prog. Ser.*, *97*, 271–285, doi:10.3354/meps097271.

Francois, R., S. Honjo, R. Krishfield, and S. Manganini (2002), Factors controlling the flux of organic carbon to the bathypelagic zone of the ocean, *Global Biogeochem. Cycles*, *16*(4), 1087, doi:10.1029/2001GB001722.

Franks, P. J. S. (1995), Thin layers of phytoplankton: A model of formation by near-inertial wave shear, *Deep Sea Res., Part I*, *42*(1), 75–91, doi:10.1016/0967-0637(94)00028-Q.

Fritz, J. J. (1999), Carbon fixation and coccolith detachment in the coccolithophore Emiliania huxleyi in nitrate-limited cyclostats, *Mar. Biol. Berlin*, *133*, 509–518, doi:10.1007/s002270050491.

Fritz, J. J., and W. M. Balch (1996), A coccolith detachment rate determined from chemostat cultures of the coccolithophore *Emiliania huxleyi*, *J. Exp. Mar. Biol. Ecol.*, *207*, 127–147, doi:10.1016/S0022-0981(96)02633-0.

Gardner, W. D., S. P. Chung, M. J. Richardson, and I. D. Walsh (1995), The oceanic mixed-layer pump, *Deep Sea Res.*, *42*, 757–775, doi:10.1016/0967-0645(95)00037-Q.

Gardner, W. D., J. S. Gundersen, M. J. Richardson, and I. D. Walsh (1999), The role of seasonal and diel changes in mixed-layer depth on carbon and chlorophyll distributions in the Arabian Sea, *Deep Sea Res., Part II*, *46*(8–9), 1833–1858, doi:10.1016/S0967-0645(99)00046-6.

Gordon, H. R., and A. Y. Morel (1983), *Remote Assessment of Ocean Color for Interpretation of Satellite Visible Imagery: A Review*, 114 pp., Springer, New York.

Gordon, H. R., O. B. Brown, R. H. Evans, J. W. Brown, R. C. Smith, K. S. Baker, and D. K. Clark (1988), A semianalytic radiance model of ocean color, *J. Geophys. Res.*, *93*, 10,909–10,924, doi:10.1029/JD093iD09p10909.

Haury, L. R., H. Yamazaki, and E. C. Itsweire (1990), Effects of turbulent shear flow on zooplankton distribution, *Deep Sea Res.*, *37*(3), 447–461, doi:10.1016/0198-0149(90)90019-R.

Holligan, P. M., M. Viollier, D. S. Harbout, P. Camus, and M. Champagne-Philippe (1983), Satellite and ship studies of coccolithophore production along a continental shelf edge, *Nature*, *304*(5924), 339–342, doi:10.1038/304339a0.

Holligan, P. M., W. M. Balch, and C. M. Yentsch (1984), The significance of subsurface chlorophyll, nitrite and ammonium maxima in relation to nitrogen for phytoplankton growth in stratified waters of the Gulf of Maine, *J. Mar. Res.*, *42*, 1051–1073.

Holligan, P. M., et al. (1993), A biogeochemical study of the coccolithophore, *Emiliania huxleyi*, in the North Atlantic, *Global Biogeochem. Cycles*, *7*(4), 879–900, doi:10.1029/93GB01731.

Honjo, S. (1976), Coccoliths: Production, transportation and sedimentation, *Mar. Micropaleontol.*, *1*, 65–79, doi:10.1016/0377-8398(76)90005-0.

Itsweire, E. C., and T. Osborn (1988), Microstructure and vertical velocity shear distribution in Monterey Bay, in *Small-Scale Turbulence and Mixing in the Ocean*, edited by J. C. J. Nihoul and B. M. Jamart, pp. 213–227, Elsevier, Amsterdam.

Itsweire, E. C., T. R. Osborn, and T. P. Stanton (1989), Horizontal distribution and characteristics of shear layers in the seasonal thermocline, *J. Phys. Oceanogr.*, *19*, 301–321, doi:10.1175/1520-0485(1989)019<0301:HDACOS>2.0.CO;2.

Itsweire, E. C., J. R. Koseff, D. A. Briggs, and J. H. Ferziger (1993), Turbulence in stratified shear flows: Implications for interpreting shear-induced mixing in the ocean, *J. Phys. Oceanogr.*, *23*, 1508–1523, doi:10.1175/1520-0485(1993)023<1508:TISSFI>2.0.CO;2.

JGOFS (1996), *Protocols for the Joint Global Ocean Flux Study (JGOFS) Core Measurements*, 170 pp., Sci. Comm. on Oceanic Res., Int. Counc. of Sci. Unions, Intergov. Oceanogr. Commiss., Bergen, Norway.

Karabashev, G. S., and A. N. Solov'yev (1978), Relation between the fluorescence maxima of phytoplankton pigments and the location of the seasonal pycnocline, *Oceanology, Engl. Transl.*, *18*, 468–471.

Kierstead, H., and L. B. Slobodkin (1953), The size of water masses containing plankton blooms, *J. Mar. Res.*, *12*, 141–147.

Kolmogorov, A. N. (1941), The local structure of turbulence in incompressible viscous fluid for very large Reynolds number, *C. R. Acad. Sci. USSR*, *30*(4), 310–315.

Lorenzen, C. J. (1966), A method for the continuous measurement of in vivo chlorophyll concentration, *Deep Sea Res., Part I*, *13*, 223–227.

Lorenzen, C. J. (1967), Vertical distribution of chlorophyll and phaeopigments: Baja California, *Deep Sea Res., Part I*, *14*, 735–745.

McManus, M. A., et al. (2003), Characteristics, distribution and persistence of thin layers over a 48 hour period, *Mar. Ecol. Prog. Ser.*, *261*, 1–19, doi:10.3354/meps261001.

McNeil, C. L., and D. M. Farmer (1995), Observations of the influence of diurnal convection on upper ocean dissolved gas measurements, *J. Mar. Res.*, *53*, 151–169, doi:10.1357/0022240953213313.

Milliman, J., P. J. Troy, W. Balch, A. K. Adams, Y.-H. Li, and F. T. MacKenzie (1999), Biologically mediated dissolution of calcium carbonate above the chemical lysocline?, *Deep Sea Res., Part I*, *46*, 1653–1669, doi:10.1016/S0967-0637(99)00034-5.

Mobley, C. D. (1994), *Light and Water: Radiative Transfer in Natural Waters*, 592 pp., Academic, San Diego, Calif.

Morel, A., and Y. Ahn (1990), Optical efficiency factors of free-living marine bacteria: Influence of bacterioplankton upon the optical properties and particulate organic carbon in oceanic waters, *J. Mar. Res.*, *48*, 145–175, doi:10.1357/002224090784984632.

Morel, A., and Y. Ahn (1991), Optics of heterotrophic nanoflagellates and ciliates: A tentative assessment of their scattering role in oceanic waters compared to those of bacterial and algal cells, *J. Mar. Res.*, *49*, 177–202, doi:10.1357/002224091784968639.

Morse, J. W., D. K. Gledhill, and F. J. Millero (2003), $CaCO_3$ precipitation kinetics in waters from the Great Bahama Bank: Implications for the relationship between bank hydrochemistry and whitings, *Geochim. Cosmochim. Acta*, *67*(15), 2819–2826, doi:10.1016/S0016-7037(03)00103-0.

Mueller, J. L., R. W. Austin, A. Morel, G. S. Fargion, and C. R. McClain (2003a), *Introduction, Background, and Conventions*, vol. I, 50 pp., Goddard Space Flight Cent., Greenbelt, Md.

Mueller, J. L., et al. (2003b), *Radiometric Measurements and Data Analysis Protocols*, vol. III, 78 pp., Goddard Space Flight Cent., Greenbelt, Md.

Mueller, J. L., C. Pietras, S. B. Hooker, R. W. Austin, M. Miller, K. D. Knobelspiesse, R. Frouin, B. Holben, and K. Voss (2003c), *Ocean Optics Protocols for Satellite Ocean Color Sensor Validation, Revision 4, Volume II: Instrument Specifications, Characterization, and Calibration*, Goddard Space Flight Cent., Greenbelt, Md.

Okubo, A. (1978), Horizontal dispersion and critical scales for phytoplankton patches, in *Spatial Pattern in Plankton Communities*, edited by J. H. Steele, pp. 21–42, Plenum Press, New York.

Osborn, T. (1998), Fine structure, microstructure and thin layers, *Oceanography*, *11*, 36–43.

Pingree, R. D. (1978), Mixing and stabilization of phytoplankton distributions on the northwest European continental shelf, in *Spatial Patterns in Plankton Communities*, edited by J. H. Steele, pp. 181–220, Plenum Press, New York.

Pingree, R. D., P. R. Pugh, P. M. Holligan, and G. R. Forster (1975), Summer phytoplankton blooms and red tides along tidal fronts in the approaches to the English Channel, *Nature*, *258*, 672–677, doi:10.1038/258672a0.

Richardson, L. F. (1926), Atmospheric diffusion shown on a distance-neighbour graph, *Proc. R. Soc. London*, *110*, 709–727, doi:10.1098/rspa.1926.0043.

Riley, G. A., H. Stommel, and D. F. Bumpus (1949), Quantitative ecology of the plankton of the western North Atlantic, *Bull. Bingham Oceanogr. Collect.*, *12*, 1–169.

Rines, J. E. B., P. L. Donaghay, M. M. Dekshenieks, J. M. Sullivan, and M. S. Twardowski (2002), Thin layers and camouflage: Hidden Pseudo-nitzschia spp. (Bacillariophyceae) populations in a fjord in the San Juan Islands, Washington, USA, *Mar. Ecol. Prog. Ser.*, *225*, 123–137, doi:10.3354/meps225123.

Robbins, L. L., and P. L. Blackwelder (1992), Biochemical and ultrastructural evidence for the origin of whitings: A biologically induced calcium carbonate precipitation mechanism, *Geology*, *20*(5), 464–468, doi:10.1130/0091-7613(1992)020<0464:BAUEFT>2.3.CO;2.

Sarmiento, J. L., G. Thiele, R. M. Key, and W. S. Moore (1990), Oxygen and nitrate new production and remineralization in the North Atlantic subtropical gyre, *J. Geophys. Res.*, *95*(C10), 18,303–18,315, doi:10.1029/JC095iC10p18303.

Scott, J. T., G. E. Myer, R. Stewart, and E. G. Walther (1969), On the mechanism of Langmuir circulations and their role in epilimnion mixing, *Limnol. Oceanogr.*, *14*, 493–503.

Sheldon, R. W., A. Prakash, and J. W. H. Sutcliffe (1972), The size distribution of particles in the ocean, *Limnol. Oceanogr.*, *17*, 327–340.

Skellam, J. G. (1951), Random dispersal in theoretical populations, *Biometrika*, *38*, 196–218.

Stanton, T. P., C. S. Law, and A. J. Watson (1998), Physical evolution of the IronEx-I open ocean tracer patch, *Deep Sea Res., Part II*, *45*, 947–975, doi:10.1016/S0967-0645(98)00018-6.

Steele, J. H., and C. S. Yentsch (1960), The vertical distribution of chlorophyll, *J. Mar. Biol. Assoc. U. K.*, *39*, 217–226.

Stommel, H. (1949), Horizontal diffusion due to oceanic turbulence, *J. Mar. Res.*, *8*(3), 199–225.

Stramski, D., and D. A. Kiefer (1991), Light scattering by microorganisms in the open ocean, *Prog. Oceanogr.*, *28*(4), 343–383, doi:10.1016/0079-6611(91)90032-H.

Strickland, J. D. H. (1968), A comparison of profiles of nutrient and chlorophyll concentrations taken from discrete depths and by continuous recording, *Limnol. Oceanogr.*, *13*, 388–391.

Tyrrell, T., and A. Merico (2004), *Emiliania huxleyi*: Bloom observations and the conditions that induce them, in *Coccolithophores: From Molecular Processes to Global Impact*, edited by H. R. Thierstein and J. R. Young, pp. 75–97, Springer, Berlin.

Yentsch, C. (1962), Measurement of visible light absorption by particulate matter in the ocean, *Limnol. Oceanogr.*, *7*(2), 207–217.

W. M. Balch, B. C. Bowler, and D. T. Drapeau, Bigelow Laboratory for Ocean Sciences, P.O. Box 475, West Boothbay Harbor, ME 04575, USA. (bbalch@bigelow.org)

A. J. Plueddeman, Woods Hole Oceanographic Institution, Woods Hole, MA 02543, USA.